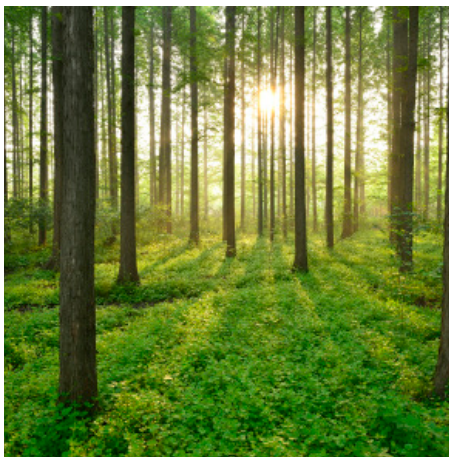
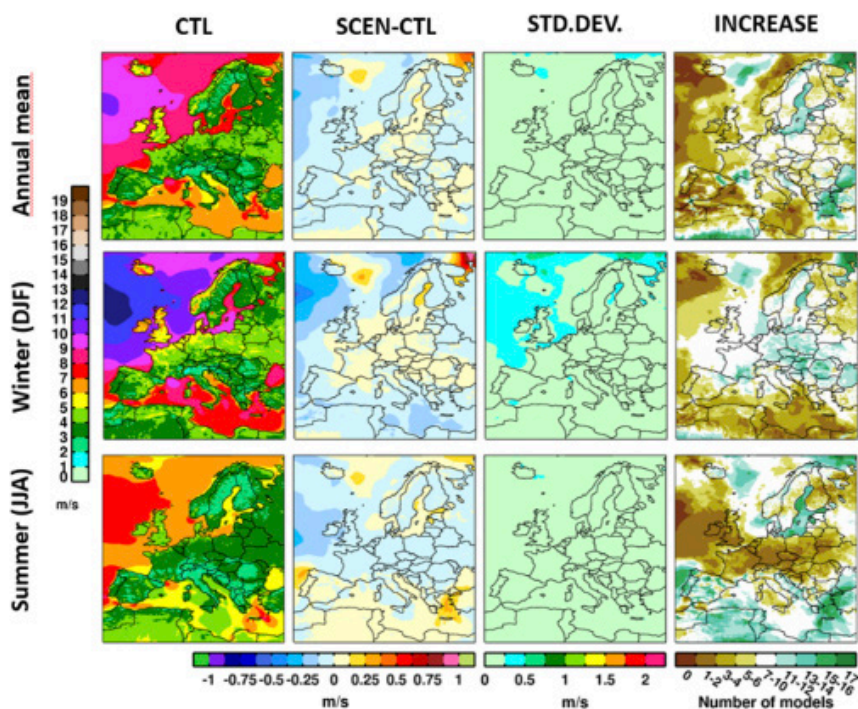


# IMPACT OF CLIMATE CHANGE ON WIND POWER IN SWEDEN

REPORT 2023:949



IMPACT OF CLIMATE CHANGE ON WIND POWER



# Impact of climate change on wind power in Sweden

ERIK KJELLSTRÖM, PETER BLOMQVIST, RAMÓN FUENTES FRANCO, LISA GÖRANSSON,  
WAHEED IQBAL, PETTER LIND AND ELENA MALZ

ISBN 978-91-7673-949-5 | © Energiforsk June 2023

Energiforsk AB | Phone: 08-677 25 30 | E-mail: [kontakt@energiforsk.se](mailto:kontakt@energiforsk.se) | [www.energiforsk.se](http://www.energiforsk.se)

## Foreword

The global emissions of greenhouse gases continue to increase, and we are moving towards a global temperature increase of more than three degrees towards the end of the century, unless we succeed in breaking the trend. The change in the earth's average temperature has a major impact on Sweden's climate, with changed climate zones, changed precipitation patterns, impact on snow conditions, higher water temperatures, etc.

This in turn affects the energy system in several ways. The energy system's vulnerability is increasing and the production conditions for different types of energy may change. The purpose of this project has been to increase knowledge of how climate change affects the future wind climate in Sweden and thus the production capacity of Swedish wind power.

In the project, Energiforsk has engaged a team of researchers and analysts from SMHI, Chalmers and Profu to deepen the knowledge about the impact of climate change on Swedish wind power. Energiforsk would like to extend a big thank you to participating researchers and to participants in the project's reference group. Furthermore, Energiforsk would like to express a big thank you to the project's financiers, namely the Swedish Energy Agency, Enercon, EON, Ellevio, Fortum, Karlstads Energi, OX2, Skellefteå Kraft, Statkraft, Svenska kraftnät and Vasa Vind

These are the results and conclusions of a project, which is part of a research programme run by Energiforsk. The author/authors are responsible for the content.

## Summary

**Analysis has been made of how the wind climate in recent decades is linked to variations in the large-scale atmospheric circulation. Also, the performance of a high-resolution climate model has been assessed. It has also been investigated how future wind conditions may change, both in the high-resolution model, but also in large ensembles of global and regional climate model simulations. In addition, an energy systems model has been applied to investigate how a future energy system including an increased fraction of wind power could be optimized to handle variations in wind between years.**

The results show that the variability in the historical wind climate can be linked to the large-scale atmospheric circulation and that this can be used to categorize different years, both in terms of total wind resource and conditions for periods with low wind speeds. Despite a large interannual variability in wind, the aggregated wind resource across Northern Europe is relatively robust. This is a result of dispersing the wind turbines geographically and thereby equalizing the production. In an example, we show that the variation in expected annual electricity production is reduced from about  $\pm 15\%$  for individual wind farms to about  $\pm 7\%$  in total if the wind power is spread over northern Europe.

The high-resolution model shows good agreement with wind observations in Sweden. Unlike models with a coarser resolution, this also applies to areas with complex topography, such as the Scandes. Scenarios for the future, where the regional model is driven by two different global models, show different future changes in the wind climate, with one scenario showing only small changes, while the other shows a clear increase in the wind resource for the studied 20-year periods. In both cases, the model shows reduced risk for ice formation, as the cold season becomes shorter. During the cold season, however, there is an increased risk of ice formation in northern areas.

Large ensembles with climate simulations show, on average, relatively small future changes in the wind resource in Northern Europe. The only clear systematic change that emerges is a reduction of a few percent in average wind speed during the summer over parts of Northern Europe. However, the absence of systematic trends does not mean that there cannot be changes and/or variations also on decadal time scales in the future as the natural variability is large.

The energy system model shows that a future energy system with a greater proportion of wind power is relatively robust against interannual variability in the wind resource. The results show that it is cost-effective to meet the electricity demand in Scandinavia with the expansion of wind and solar supplemented with the existing hydropower.

## Keywords

Climate change, climate scenarios, climate modelling, wind power, energy system modelling

Klimatförändring, klimatscenarier, klimatmodellering, vindkraft, energisystemmodellering

## Sammanfattning

**Hur vindklimatet kan kopplas till variationer i den storskaliga atmosfäriska cirkulationen har undersökts för de senaste decennierna. En högupplöst regional klimatmodell har utvärderats. Framtida förändringar i klimatet har undersökts, dels i den högupplösta klimatmodellen och dels i stora ensembler med globala och regionala klimatmodeller. Vidare har en energisystemmodell använts för att undersöka hur ett framtida energisystem, med kraftigt utbyggd vindkraft, kan optimeras för att hantera variationer i vindresursen från ett år till nästa.**

Resultaten visar att variabiliteten i det historiska vindklimatet kan kopplas till den storskaliga atmosfärscirkulationen och att detta kan användas för att kategorisera olika år, både den totala vindresursen och förutsättningar för perioder med låga vindhastigheter. Generellt syns en stor variabilitet mellan år. Trots detta är den sammanlagrade vindresursen över hela Nordeuropa relativt robust till följd av utjämnningseffekten som uppstår då vindkraftverken är geografiskt utspridda. Vi visar i ett exempel på att variationen i förväntad årlig elproduktion minskar från ca  $\pm 15\%$  för enskilda vindkraftsparker till ca  $\pm 7\%$  totalt om vindkraften sprids över norra Europa.

Den högupplösta modellen visar på bra överensstämmelse med observationer av vindhastigheter i Sverige. Till skillnad från modeller med grövre upplösning gäller detta inte minst för områden med komplex topografi, som skandinaviska fjällkedjan. Scenarierna, där den regionala modellen drivs av olika globala modeller, visar på olika framtida förändringar i vindklimatet. I det ena fallet syns relativt små förändringar medan det andra fallet ger en tydlig ökning i vindresursen för de studerade 20-årsperioderna. I båda fallen visar modellen på generellt minskad risk för isbildning då den kalla säsongen blir kortare. Under den kalla säsongen syns dock en ökad risk för isbildning i norr.

Stora ensembler med många klimatsimuleringar visar i medeltal på relativt små framtida förändringar i vindresursen i Nordeuropa men också på en stor variabilitet med stora skillnader mellan år och årtionden i enskilda modellerna. Den enda tydliga systematiska förändringen som framträder är en viss minskning av medelvindhastigheten under sommaren över delar av Nordeuropa. Frånvaron av systematiska trender innebär inte att det inte kan komma att ske förändringar framöver då den naturliga variabiliteten är stor.

Energisystemmodelleringen visar att ett framtida energisystem med en större andel vindkraft är relativt robust mot mellanårsvariabilitet i vindresursen. Resultaten visar att det är kostnadseffektivt att möta elbehovet i Skandinavien med utbyggnad av vind och sol kompletterat med den existerande vattenkraften.

## List of content

<b>1</b>	<b>Introduction and background</b>	<b>8</b>
1.1	Wind power in the energy system in a changing climate	8
1.2	Changing wind conditions in a changing climate	9
1.3	Aim of this study	12
<b>2</b>	<b>Methods and data</b>	<b>13</b>
2.1	Historical weather data	13
2.2	Climate model data	15
2.3	Analysed climate change indicators	16
2.4	Circulation types	17
2.5	Energy system model	18
<b>3</b>	<b>Results</b>	<b>21</b>
3.1	Wind and Wind power variability in Northern Europe	21
3.2	Circulation types	26
3.3	Evaluation of the regional climate model HCLIM	29
3.4	Changes in the wind climate in HCLIM	35
3.5	Changes in icing conditions in HCLIM	44
3.6	Changes in the large-scale circulation and in circulation types	45
3.7	The energy system and its link to circulation types	48
<b>4</b>	<b>Discussion</b>	<b>55</b>
4.1	Representativity of models	55
4.2	Impacts of climate change on the energy system	56
<b>5</b>	<b>Conclusions</b>	<b>58</b>
<b>6</b>	<b>References</b>	<b>60</b>
<b>7</b>	<b>Appendix</b>	<b>64</b>
7.1	GIS parameters for onshore / offshore wind power	64
7.2	Technology data for the Energy System model	66

# 1 Introduction and background

## 1.1 WIND POWER IN THE ENERGY SYSTEM IN A CHANGING CLIMATE

Global warming is rapid and global mean temperature is now more than 1.1°C warmer compared to preindustrial conditions (WMO, 2023). Human-induced emissions of greenhouse gases is the main cause of this change (IPCC, 2021) with impacts on ecosystems and society in all continents (IPCC, 2022a). To avoid even stronger impacts in the future, rapid and strong mitigation is required. In this context, renewable energy sources, such as wind power, plays an important role in all modelled pathways for keeping global warming under 2°C above preindustrial conditions (IPCC, 2022b).

A fundamental consideration in planning the future energy system is therefore to address under which future climate conditions wind power will operate. Importantly, wind power is directly impacted by global warming through changes in wind speed and how it translates to changes in wind power generation. Other changes in climatological conditions, such as conditions for icing of wind turbines, may also come into play. In addition, climate change also has secondary effects on wind power in three important ways; i) by incentivizing climate change mitigation, ii) by changing the conditions for other electricity generation options, and iii) by changing the demand for electricity for heating and cooling purposes.

Climate mitigation and the shift towards a carbon neutral electricity system has a large impact on the role of wind power in the energy system. An expected consequence of climate mitigation in Sweden is a substantial increase in electricity demand for the electrification of the industry and transport sector (Energimyndigheten, 2023). Due to the cost-competitiveness of wind power in northern Europe relative to other electricity generation technologies associated with low emissions of carbon dioxide, wind power is expected to supply the vast majority of the upcoming demand for electricity in this region (IEA, 2022). Wind power is thus growing from a marginal electricity supplier to the main bulk provider and any changes in conditions for wind power because of a warmer climate can thus have a large impact on the future electricity supply.

Previous work has shown that a warmer climate changes both temperatures and precipitation patterns and thereby the conditions for hydropower (Scharff et al., 2023). Hydropower is impacted both in terms of an increased net inflow of water to rivers and dams on an annual basis but also in terms of more inflow of water during winter and fall and less inflow from snowmelt in the spring. Hydropower has an important role in managing variations in the electricity system since electricity generation from hydropower with storage can be planned with great flexibility. Notably, hydropower can complement wind power by producing electricity during periods with low wind speed. Recent work has shown that hydropower in Sweden can be expected to maintain this ability in a warmer climate (Scharff et al., 2023).

A warmer climate is expected to reduce the electricity demand for heating purposes. The electricity demand can thus be expected to be lower in the winter in

a warmer climate. At the same time, the demand for cooling in the summer is increasing. However, since the temperature difference between inside and outside when heating a house in winter is much larger than the temperature difference when cooling it in the summer, total electricity demand for regulating the indoor temperature can be expected to be reduced. In the Nordic countries wind power production is typically greater during the winter. Thus, in an electricity system with a warmer climate, seasonal variations in the value of electricity between summer and winter, and the need to manage seasonal variations, is reduced.

## 1.2 CHANGING WIND CONDITIONS IN A CHANGING CLIMATE

The wind climate in northern Europe is highly dependent on the large-scale atmospheric circulation, which gives rise to strong variations on scales from days and weeks to years and decades. The large decadal or multidecadal variability has been found to dominate over long-term trends in the region (Barring and von Storch, 2004; Rutgersson et al. 2015). A problem in assessing historical changes lies in inherent inhomogeneities in series of direct wind measurements (Meier, 2022). As a complement, other data can be used as proxy information to deduce past changes. An example of this is geostrophic wind speed that is derived from horizontal gradients in the mean sea level pressure. Figure 1.1 shows how the geostrophic mean wind speed has varied since 1900 in southernmost Sweden. It is clear from the figure that there have been some decades with higher and some with lower wind speed but that there are no systematic long-term trends. The figure also reveals variations from year to year of approximately  $\pm 10\%$ .

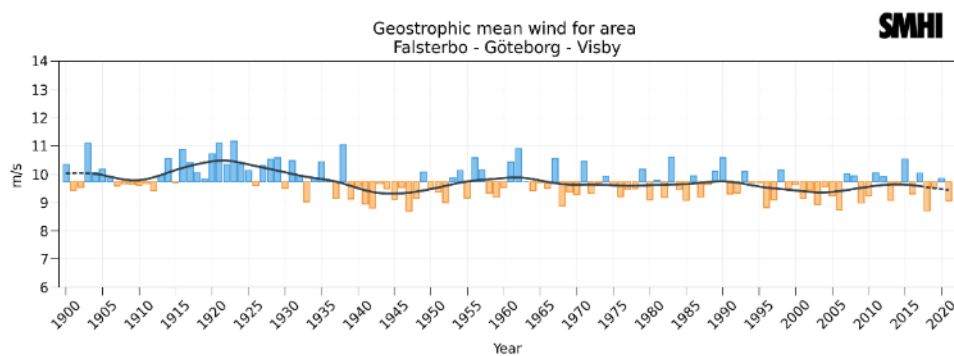


**Figure 1.1:** Average potential geostrophic wind energy derived for an area between Falsterbo-Göteborg-Visby in southern Sweden. Blue colors indicate higher number than the average for 1961-1990, orange lower. The black line shows a running mean filtering to around ten years. For more information see Schimanke et al. (2022).

Information about future climate conditions can be derived from climate projections with climate models simulating the future under different forcing scenarios. Previous work addressing future climate change and its impact on wind power in northern Europe includes Claussen et al. (2007), Hovsenius and Kjellström (2007), Claussen et al. (2011), Blomqvist et al. (2021) and Christensen et al. (2022). Common for these studies is that projected future changes in wind speed are relatively modest taken as an average over ensembles of climate model projections. Also, there is a strong dependence on which individual climate model projections and which time periods that are assessed albeit mostly without

consistent long-term trends. This illustrates that the strong variability of the wind climate seen in the historical climate is also a dominating factor for the future.

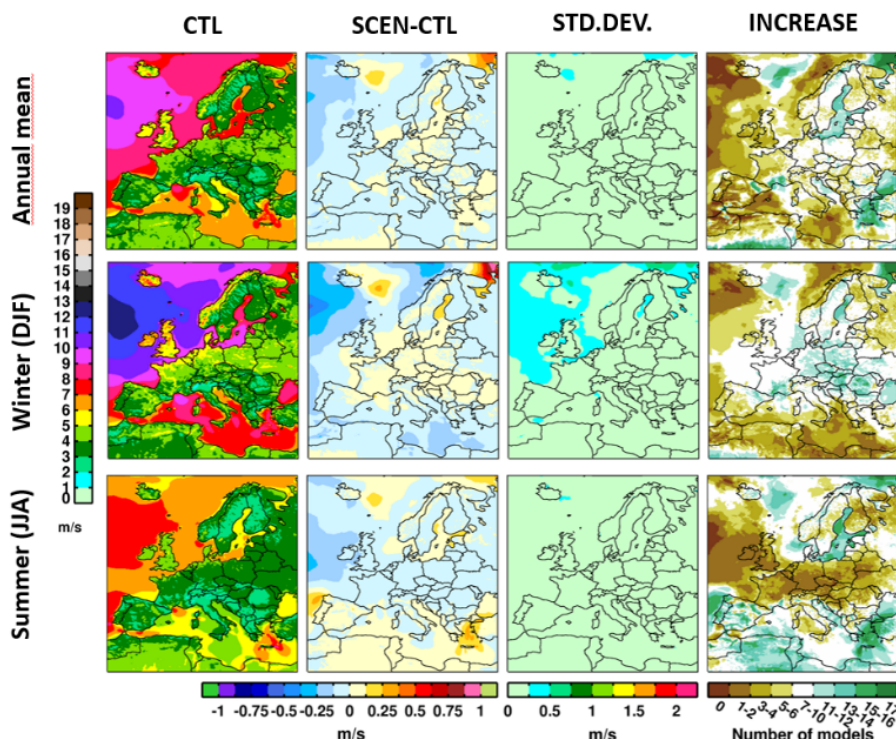


Figure 1.2: Annual mean, winter (DJF) and summer (JJA) 10-meter wind speed based on Kjellström et al. (2018). The leftmost column shows the control climate (CTL) 1971-2000, the second column from the left shows the change from 1971-2000 to the first 30-year time period when the global mean temperature in the global model reaches +2C above the 1850-1900 average. The third column shows the intermodel spread defined by the standard deviation between the ensemble members. The fourth column indicates how many out of the 17 model simulations that indicate an increase in wind speed.

Figure 1.2 shows changes in the wind climate at the time when global warming reaches +2°C in an ensemble of 17 regional climate model simulations. For the historical time period the models simulate windier conditions in winter compared to summer over most of Europe as clearly seen in the ensemble mean (leftmost column). The climate change signals (second column from the left) indicate that wind speed is projected to decrease in more areas than where it is projected to increase. Changes are relatively small and even if the spread between models (third column from the left) is small in absolute numbers there are uncertainties, especially over the North Atlantic in winter. The maps to the right indicate that some signals are relatively robust across most ensemble members. For instance, the wintertime decreases in the Mediterranean region as well as the summertime decreases over the Atlantic and central Europe are seen in most models. Notably, over northern Europe (incl. Sweden) the signal is not robust across the ensemble with some models showing increasing wind speed and others showing decreases. An exception to this is increasing wind speed over parts of the Baltic Sea. This has been assigned to warmer sea surface temperatures (and less sea ice) leading to less stable conditions in the atmosphere and thereby stronger mixing of momentum from higher levels to near the surface resulting in higher wind speed at low level.

The link between changes in wind speed (Figure 1.2) and changes in large-scale circulation can be seen by comparing also with changes in mean sea level pressure (Figure 1.3). Most of the included simulations indicate increasing mean sea level pressure in southernmost Europe in winter. Correspondingly, there is an increase in an area stretching from the British Isles eastwards towards central and Eastern Europe in summer. These are the areas and seasons where many models indicate decreasing wind speed (Figure 1.2). For northern Europe, where there is no clear indication of any such large-scale robust changes in wind speed, the models do not agree on either sign of change or magnitude of changes in the pressure pattern.

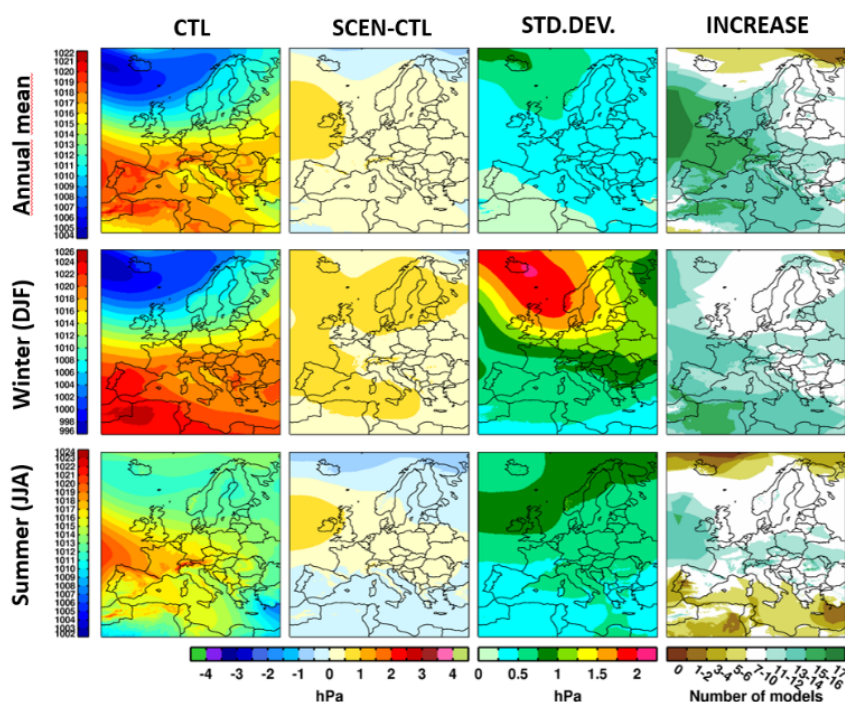


Figure 1.2: As Figure 1.2 but for mean sea level pressure.

To a large extent differences between single projections are related to natural variability (Kjellström et al. 2018). Consequently, large ensembles of climate simulations are needed to address questions of robustness and uncertainty in potential climate change (e.g., Deser et al. 2020). Another commonality between previous work is that the assessed models all have operated at relatively coarse resolution (tens to hundreds of kilometres). As high resolution is important to describe details in the landscape including orographic details, it is clear that these studies have limitations especially in high-altitude regions such as the Scandes.

Icing problems may change depending, either on changes in temperatures or moisture, or depending on combinations of changes in both. Higher temperatures in the future generally can be expected to lead to less problems with icing as less days during the year have temperatures close to or below 0°C. In some regions, however, temperatures may still be close to 0°C also in a warmer climate, which may then increase the risk of icing. It has been found that, during winter in northern Sweden increased problems with icing may occur (Blomqvist et al. 2021).

### 1.3 AIM OF THIS STUDY

This report presents results from a project on changes in wind power potential and its impacts in northern Europe with focus on the energy system in Sweden. The work comprises the following activities:

- We assess wind power potential in northern Europe over the last decade as determined by historical wind conditions.
- We evaluate climate models at different horizontal resolution in their ability to simulate details in the observed wind climate in the region in relation both to gridded data sets and individual meteorological stations as well as measurements from wind power turbines.
- We assess climate change aspects for the wind climate and the potential for wind power production based on a very high-resolution regional climate model operating at a horizontal resolution of 3 km.
- We specifically investigate how wind power production relates to different large-scale atmospheric circulation patterns and how this may change in a future warmer climate.
- We set the results of the very high-resolution regional climate model in a wider context by comparing with larger ensembles of regional and global climate models.
- We investigate impacts on the Nordic energy system based on changes in atmospheric circulation patterns and an electricity systems model.

## 2 Methods and data

Here we describe models and data used in the project. This includes different sources of historical weather used for assessing past changes/variability in the wind climate and for evaluating climate models. We also introduce the different climate models and simulations that are analysed. Various methods of treating data from models and historical weather are also describe, including those that have been introduced to facilitate comparisons between models and observations, and for describing how the wind climate can be linked to large-scale atmospheric circulation types. Finally, we describe the energy system model used for synthesizing the information.

### 2.1 HISTORICAL WEATHER DATA

We use three different types of historical weather data:

- reanalysis data,
- in-situ 10-m wind speed observations from a large number of meteorological observational stations in Sweden, and
- in-situ wind speed measurements at hub height from several wind turbines in the four energy prize areas in Sweden.

Reanalysis data, that is a blend of observational data and weather forecast model output, is taken from the global reanalysis products ERA-Interim (Dee et al. 2011), ERA5 (Hersbach et al., 2020) and MERRA (Gelaro et al. 2017). ERA5 is specifically used for providing mean sea level pressure for determination of circulation types (Ch. 3.4) and for providing weather data as input to the energy system model (Ch. 3.9). The older reanalysis data set from the European Centre for Meteorological Weather Forecasts (ECMWF) ERA-Interim is not used directly in the report here but was used as boundary conditions to the HCLIM-model used here. Wind speed at hub height, used for analysing the variability in wind power production over northern Europe (Ch 3.1) and for comparing with climate model results (Ch. 3.2), has been taken from MERRA at a one-hour resolution.

In Ch 3.2 we compare wind speed observations from SMHI's observational network with the most high-resolution regional climate model used in the project. In total 161 stations have been used as illustrated in Figure 2.1. These observations are taken at 10 m height over the ground and we have assessed daily mean values. In addition to the near surface measurements, we also use wind speed data from hub height as recorded on several operational wind turbines at ten wind farms spread over Sweden (Table 2.1) in the four different electricity price areas (Figure 2.1). These data are based on high-frequency (order of seconds) measurements and have been provided to us as averages over longer periods from 10 minutes to 1 hour. For comparison with the high-resolution climate model HCLIM (see Chapter 2.2) we use observational data at 3-hourly temporal resolution.

**Table 2.1:** Information about the wind farms from which observed wind speed data was used. The ID indicates which of the 4 electricity price areas (SE1-SE4, see Figure 2.1) each wind farm belongs to, the number of turbines for each wind farm represents those from which we received data. The hub height is where the measurements were made.

ID	Turbines	Hub height	Measurement period	Data availability
SE1.1	24	120	2016–2020	99.0%
SE1.3	22	105	2012–2018	99.4%
SE1.4	1	100	2014–2018	97.8%
SE2.1	47	95	2011–2018	99.1%
SE3.1	12	119	2013–2016	96.9%
SE3.2	4	100	2013–2018	99.5%
SE4.1	12	90	2012–2016	95.9%
SE4.2	5	80	2012–2016	99.7%
SE4.3	6	90	2012–2016	94.2%
SE4.4	8	90	2012–2016	94.7%

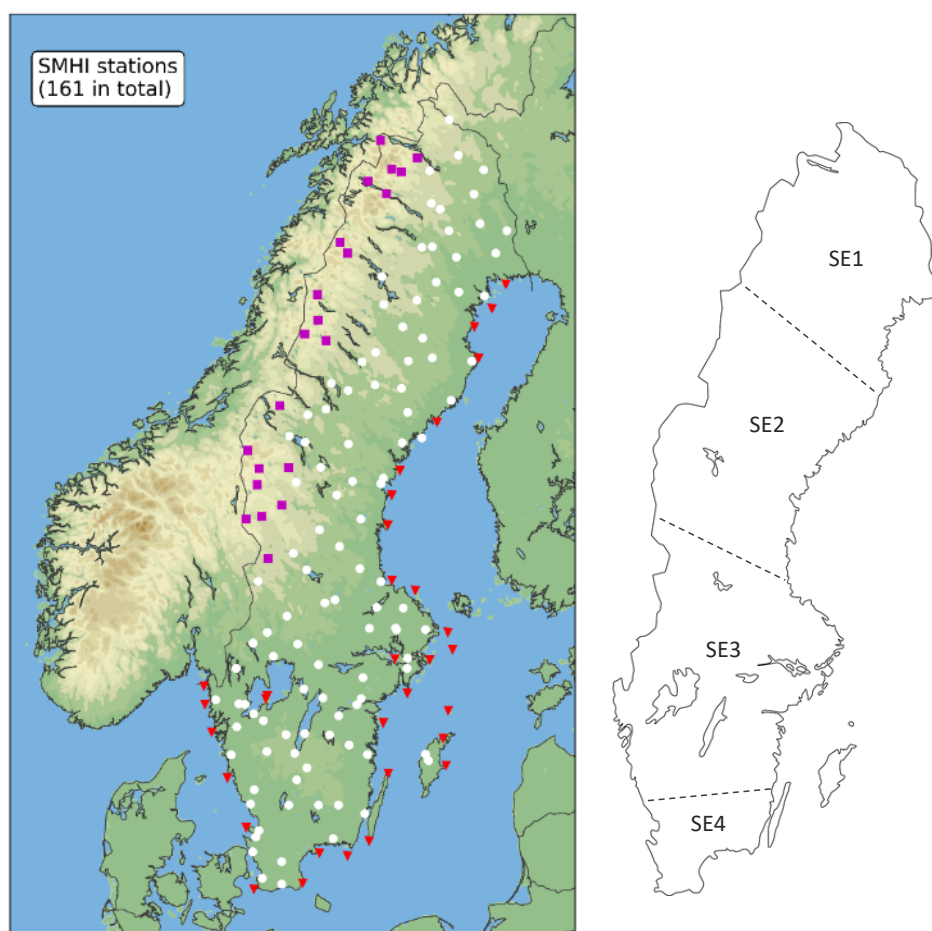


**Figure 2.1:** Location of SMHI observational stations for wind speed at 10m level above ground used in the comparison with model results. The stations are coded for different types of regions according to i) “coastal” red triangles, ii) “inland” white circles and iii) “mountains” purple square. The right panel shows the four different pricing areas (SE1-SE4) used in Sweden.

## 2.2 CLIMATE MODEL DATA

We use climate model data from different types of climate models including: i) a very high-resolution convection permitting model, ii) coarser scale regional climate models and iii) coarser scale global climate models. The very high-resolution convection permitting model is used to produce detailed maps of the wind climate in Scandinavia and how it may change in the future while the coarser scale regional and global models are used to set the results from the very high-resolution model into a wider perspective.

### *Regional climate model*

The HARMONIE-CLIMATE regional climate model (HCLIM) can be operated at different horizontal scales (Belušić et al. 2020). Here, we analyze HCLIM results from simulations undertaken at 12 and 3 km horizontal resolution. For the 12 km simulations HCLIM was forced with lateral boundary conditions, sea surface temperatures and sea-ice extent from the ECMWF reanalysis ERA-Interim and from two different global climate models under different emission scenarios for the future. The simulations with the convection permitting model version at 3 km horizontal resolution was forced by results from the HCLIM simulations at 12 km. For details see Lind et al. (2020 and 2022).

For comparisons with the data from the observational stations and from the wind farms, HCLIM data has been extracted for the nearest grid box either at the 10 m level or at 100-meter displacement height. The temporal resolution is daily (diurnal averages) for comparison at the 10 m level and as instantaneous values every three hours for comparison at the 100 m level. For these comparisons, HCLIM data was taken from the ERA-Interim driven simulation covering the full period 1998–2018. As the measurement period is shorter at the respective wind farms (cf. Table 2.1) HCLIM data was extracted for the matching years for each individual wind farm.

### *Global climate model*

To set results of the regional climate models in a wider perspective we use data from the SMHI large ensemble (S-LENS, see Wyser et al. 2021). S-LENS consists of 50 members with the global climate model EC-Earth run under different scenarios for the future. Here, we use results from the SSP5-8.5 scenario to illustrate how the large-scale circulation is projected to change.

### *Other global and regional climate models*

We also use global climate models from CMIP6 (the sixth phase of the Coupled Model Intercomparison Project, Eyring et al. (2016)) and regional models from EURO-CORDEX (Jacob et al. 2020). These ensembles are assessed via the IPCC interactive atlas (Iturbide et al., 2021 and Gutiérrez et al., 2021)<sup>1</sup>.

---

<sup>1</sup> <https://interactive-atlas.ipcc.ch/>

## 2.3 ANALYSED CLIMATE CHANGE INDICATORS

### *Wind power potential*

As an overall indicator of wind power potential, we have calculated the wind power density (WPD) at hub height using

$$WPD = 0.5 \rho v^3$$

where  $\rho$  is the density of the air and  $v$  is the wind speed at the hub height. For the climate models we have used the 100 m level to represent the hub height in all analysis.

The actual wind power production depends not only on the wind power density but also on properties of the technical aspects of the wind power turbines, which can be illustrated by power curves for the individual wind power turbines. Here, Figure 2.2 illustrates such power curves for a set of different turbines. The curves clearly show that the full power is only achieved for a certain range starting at around 8-12 m/s for the assessed turbines. For very high wind speeds there may also be limitations to the power production potential as the power plants may need to be shut down to avoid wind damages as illustrated for the Vestas V136 turbine (orange line) in the diagram. The development of wind turbines and thus their power curve has progressed rapidly, which has a large impact on the production of the wind turbines.<sup>2</sup>

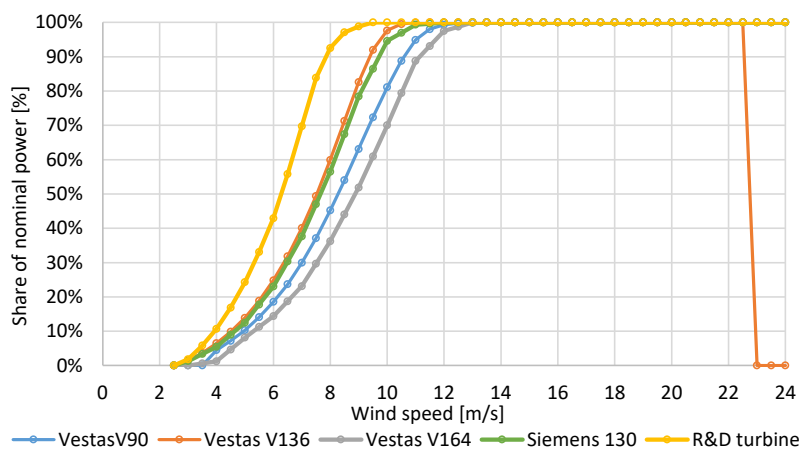


Figure 2.2: Power curves for 4 different wind turbines, and a so-called research turbine.

### *Conditions with low wind production*

An aspect that is of particular interest to the energy system is the share of days with low wind speed. We have chosen 3 wind speed levels to represent "low wind" defined by a wind speed of maximum 4.5 m/s, 5.5 m/s and 6.5 m/s respectively. These three levels have been chosen to represent what can be considered as *low wind* linked to the power curve of the wind turbines (cf. Figure 2.2). As the figure illustrates, low wind is a bit of a fluid concept since you get about 19% of nominal

<sup>2</sup> Main factors are rotor diameter and maximum power for the turbine.

power with a Vestas V164 at 6.5 m/s, while you can get about 32% with a Vestas V136. Differences in the percentages lie primarily in the relation between rotor size and the nominal power of the wind turbine.<sup>3</sup>

Note that power curves for wind turbines are normally based on 10-minute average wind speed values. Over time, the specific power, the ratio of the rotor diameter to the generator power, of wind turbines has decreased. Wisser and Bolinger (2015) found that it went from 390 W/m<sup>2</sup> to 250 W/m<sup>2</sup> for new installations in the USA in the period 1998–2014. Johansson et al. (2017) show that wind turbines with low specific power can largely compensate for areas with low average wind speed, so that a relatively high penetration level<sup>4</sup> of wind power can be reached, about 40%.

#### *Conditions with high wind production*

High wind speed implies a high potential for generating wind power. Here, we have looked at the share of days with daily average wind speed above 10 m/s. This level can be considered as defining how many full load hours (FLH) there is at a certain location. The actual FLH is a turbine specific property and we note that for some turbines 10 m/s overestimates the number of full load hours, while for others it may be an underestimate.

#### *Conditions with risk of wind damage*

At very high wind speed there is a risk of damage to wind turbines. Consequently, turbines may be shut down at very high wind speed. For the Vestas V136 turbine in Figure 2.2 this is the case at wind speed above 22 m/s. In the report we use instead a threshold of 25 m/s for instantaneous values to represent very high wind speed.

#### *Conditions with risk of icing*

To properly determine if there is a risk of icing of the wind turbines detailed information about local meteorological conditions needs to be known. Building on climate model information this involves microphysical properties of clouds, wind speed, precipitation, humidity and temperatures at the sub-grid scale (Rydblom and Thörnberg, 2020). As this information is not available as output from climate model integrations, we use a crude measure to indicate if there is a risk of icing or not based on existing model output. For the analysis presented here (Chapter 3.5), we define risk of icing when the temperature at hub height is less than 0°C and the cloud liquid water content is higher than  $0.5 \cdot 10^{-4}$ .

## 2.4 CIRCULATION TYPES

That large-scale atmospheric circulation strongly determines the weather conditions in northern Europe is clear. In a study using a clustering method to categorize situations depending on large-scale atmospheric pressure patterns, Kjellström et al. (2022) show that observed changes in Swedish daily and monthly

<sup>3</sup> The Vestas V136 has a nominal power of 3.5 MW while the Vestas V164 has nominal power of 8.0 MW.

<sup>4</sup> The penetration level refers to the percentage of electricity generated by a particular resource.

mean temperature and precipitation from 1961-1990 to 1991-2020 can partly be attributed to changes in the frequency of different circulation types between the two time periods. Such differences would naturally also have direct impact on the wind climate due to the strong differences between high-pressure situations with generally low wind speed and low-pressure dominated weather with generally stronger winds. Categorizing weather situations according to such large-scale atmospheric circulation patterns is a commonly used metric to simplify meteorological variability. It has also been used to explain some of the day-to-day variability in variables relevant for renewable energy production, such as wind speed and solar radiation (van der Wiel et al. 2019).

Here, we apply the SANDRA method as also used in Kjellström et al. (2022). SANDRA (the simulated annealing and diversified randomization classification scheme) is a clustering technique that attempts to minimize the sum of Euclidian distances within a class while at the same time maximizing the distances between the classes. As input to SANDRA we use daily mean sea level pressure fields from ERA5. Here, anomalies are used as this was shown to improved the performance of the scheme by Hansen and Belušić (2021). Clustering with SANDRA can be done into an optional number of categories. Here, we set this number to ten and perform the clustering for all days in the 1986-2005 period.

## 2.5 ENERGY SYSTEM MODEL

The potential annual production of wind power, typically expressed as the full load hours, and its distribution over time determines the cost-competitiveness of wind power relative other electricity generation technologies and the role of wind power in the electricity system. Any alterations in wind conditions due to climate change could therefore potentially translate to changes in electricity system composition and operation.

To investigate the impact of changes in wind conditions from a warmer climate on the electricity system the following steps were taken;

- 1) An electricity system investment model was applied to investigate the cost-optimal electricity system composition in the Nordic countries using weather data from ten different historical years.
- 2) The prevalence of different circulation types for the ten historical years was assessed.
- 3) The impact of a warmer climate on the prevalence of different circulation types was analysed.
- 4) Combining the understanding of the impact of circulation types on electricity system composition (from steps 1-2) with the knowledge of the impact of a warmer climate on prevalence of circulation types (step 3) the impact of a warmer climate on the cost-optimal electricity system composition was estimated.

The electricity system model applied in this work is based on (Göransson et al. 2017 and Johansson et al. 2020). It optimizes the fraction of different electricity

producing types in the energy system. This is achieved by minimizing the total cost of meeting the demand for electricity and district heating every hour for a given year, including annualized investment costs as well as cost of operation.

The model is set up covering Sweden, Norway, Denmark and Finland subdivided into ten regions (see Figure 2.3). The regional subdivision represents major bottlenecks in the transmission grid. Within each region, the demand for electricity and district heating has to be met each hour. Exchange of electricity between regions is allowed as long as it is within the limitations of the transmission grid.

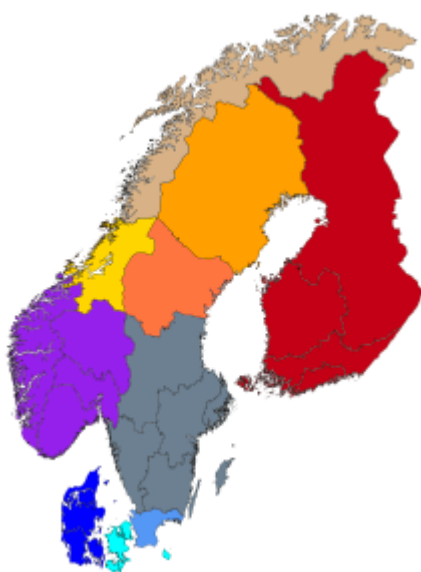


**Figure 2.3.** Regions used in the energy system model in this study. The polygons defined for the four areas in Sweden regions differ slightly from the more simplified ones used for illustration in Figure 2.1. Neither of the two exactly follows the four electricity price areas in Sweden, but we refer to them as SE1 to SE4 (starting from the north) in the following. The Danish areas are referred to as DK1 (east) and DK2 (west) and the Norwegian areas NO1 (south) to NO3 (north).

The energy system model includes a range of electricity generation investment options including onshore and offshore wind power, solar photovoltaic, biomass and biogas combined heat and power, nuclear power, biogas combined-cycle gas turbines and biogas open-cycle gas turbines. Biomass and biogas combined heat and power can also be used to supply the need for district heating together with electric boilers and heat pumps. The model also allows to invest in storage options such as batteries and tank heat storages. For wind power, we use two classes for onshore wind. These represent wind power in respectively wind class 4 representing good wind conditions (WONA4) and wind class 5 representing very good wind conditions (WONA5).

The calculations are applied to year 2045 in terms of constraints on emissions of carbon dioxide and technology costs, with an hourly resolution. Costs for the technology options are based on IEA World Energy Outlook (IEA, 2022) and the report on Technology data published by the Danish Energy Agency (DNA, 2016) and can be found in appendix 7.2. It is assumed that the existing hydropower and transmission grid capacity as of today remains unchanged in 2045. Weather

dependent data for wind speed, solar insolation and temperature, are taken from ERA5 for ten different historical years between 1999-2018. The years are chosen to represent different prevalence of the large-scale atmospheric circulation types, to capture the impact of variations in atmospheric circulation on the cost-optimal electricity system composition.

In order to study the actual wind power availability, the grid point wise wind data needs to be processed. For this transformation the study uses the Global energy GIS model, designed for energy system studies by Mattsson et al. (2021). The model transforms renewable resource data, such as wind data, to power time-series and energy capacity availability. For wind power, a wind farm power curve is applied to the available wind data for each grid point and each time step. The wind farm power curve used in here is aligned to the power curve of the Siemens Gamesa G114 2.1 MW wind turbine as described in Appendix 7.1. As all land area is not available for wind power production, auxiliary GIS data sets are used to reduce the data to utilizable land area. By now there is still a large number of available grid points with individual wind power time-series. The large inter-connection of sites via power cables, creates a power smoothing over large areas. In the energy system model applied, production and consumption are balanced within one region. It is possible to trade electricity between regions. Import and export of electricity between regions is limited by the capacity of the transmission grid. This assumption smooths the power production throughout larger areas and results in modelled power timeseries that are aggregated within the electricity regions, visible in Fig. 2.3. For each of the ten electricity regions, the aggregation creates five different power time-series, representing five different wind classes, defined in the Appendix 7.1. The translation from ERA 5 wind speeds to wind power production in the energy system models using the Global Energy GIS model is further detailed in the Appendix 7.2.

## 3 Results

### 3.1 WIND AND WIND POWER VARIABILITY IN NORTHERN EUROPE

As wind speed is highly variable in space and time it is not possible to plan the wind power production in detail. In this section we describe variations in wind speed and wind production potential in northern Europe for the period 2010-2020. The results are drawn from a background report in Swedish (Blomqvist et al. 2023) investigating variability, smoothing effects and other aspects as described below.

Since the power curve of wind turbine is far from linear, but rather have the form shown in **Fel! Hittar inte referensköll.** above, we chose to focus on the variation in potential power output from the windfarms instead of the wind speed variation. The analysis focusses on how wind power production varies across northern Europe over time, which aims to provide a better insight into what the variation means and thus a foundation for how it can be managed. There have been some studies on how wind power varies in northern Europe and what the geographical spread of wind farms means (Reichenberg, 2014; 2017; Olausson, 2016; Holttinen, 2003). In the slightly older study by Holttinen (2003), measurement data for 2000–2001 from a large number of wind farms in Finland (21), Sweden (6), Norway (6) and Denmark (hundreds) were used. Holttinen shows that there is an equalizing effect of wind power being geographically dispersed. Reichenberg et al. (2014) shows a method to reduce the effects of wind power variations in electricity production by optimizing the location of new wind farms in the Nordic countries plus Germany. They show that it is possible to reduce the variations significantly by considering both the capacity factor of the wind turbines and the variation factor, i.e. how the wind varies in relation to other areas, to achieve the best results. Olausson (2016), in turn, argues that it is important to consider the wind turbines' improved performance (increasing capacity factor) as it contributes to reducing variation in electricity production.

In the background report, Blomqvist et al. (2023) show that MERRA-data is a useful basis for carrying out the analyses in this part. MERRA-data at a height of 120 meters was used and applied at a turbine that is reasonably representative of wind turbines being constructed today, see the power curve for Siemens 130 in Figure 2.2 (other turbine brands have similar power curves such as Enercon, Vestas or Nordex). The aim was to focus on the variation and smoothing arising from the wind conditions being different between different geographic locations, which is why we did not adapt the turbine selection according to what is suitable for each specific location, but instead used the same standard turbine for all locations. This focus on the contribution of the wind speed also meant that we did not consider unavailability of the turbines.

To study production characteristics in detail, we have looked at wind availability, hour by hour, from 2010 to 2020 for wind capacities in a total of 51 locations in northern Europe (**Fel! Hittar inte referensköll.**). The capacities used in each location has been based on European and national data and estimations, for example the Swedish Energy agency, the Norwegian Water Resources and Energy Directorate, the Danish Energy Agency, and Wind Europe. Table 3.1, which

summarizes the assumed capacities, shows that the capacity becomes more dispersed over the years.

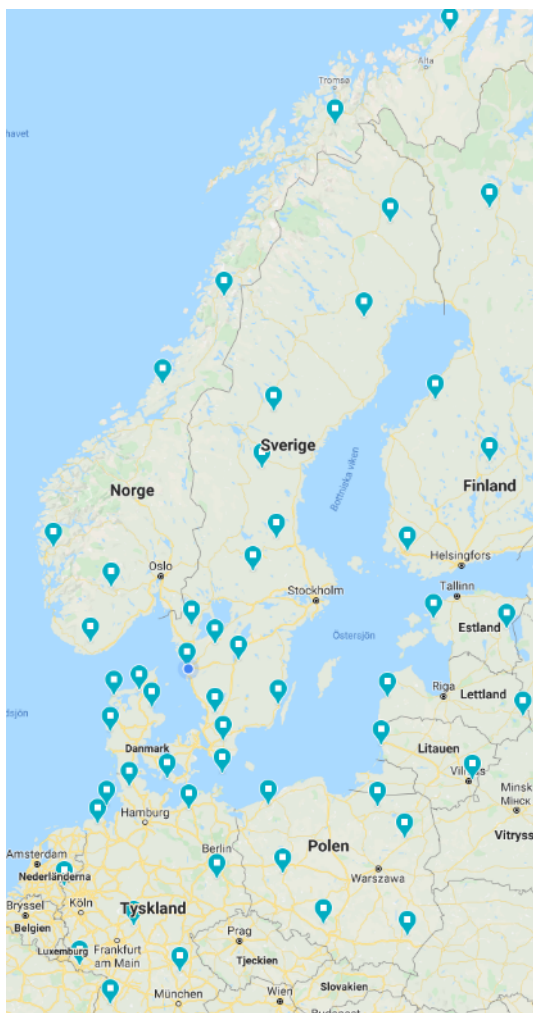
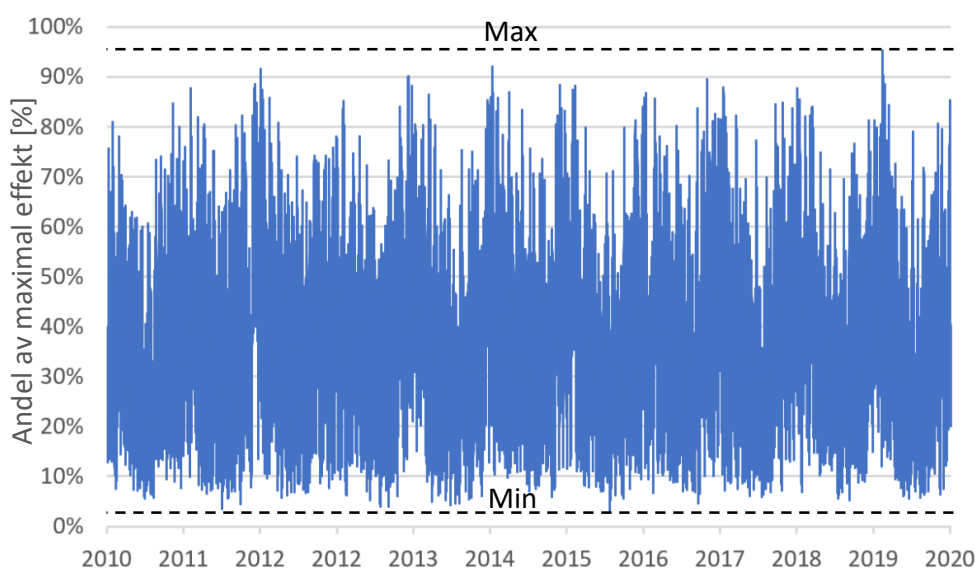


Figure 3.1: Map over locations of assumed wind farms.

Table 3.1: Installed capacity per country in GW and as a share of total capacity.

Country	Installed capacity 2019 [GW]	Installed capacity 2030 [GW]	Share of total capacity 2019	Share of total capacity 2030
Sweden	8.9	30.1	10.0%	15.1%
Norway	2.6	12.9	2.9%	6.5%
Denmark	6.1	12.0	6.8%	6.0%
Finland	2.0	10.0	2.3%	5.0%
Germany	62.1	105.4	70.0%	52.8%
Poland	6.4	26.4	7.2%	13.2%
Estonia	0.3	1.4	0.3%	0.7%
Latvia	0.4	1.1	0.4%	0.5%
Lithuania	0.0	0.5	0.0%	0.2%

In **Fel! Hittar inte referenskälla.2**, the hourly total electricity production from wind power in Northern Europe for 2010-2020 is shown, based on the wind power fleet according to Table 3.1 and **Fel! Hittar inte referenskälla.** The figure shows that the aggregation of all production never reaches the sum of the total installed capacity, instead the maximum electricity production is 95%. In the same way the total electricity production is never zero, but at least at about 3% of the installed capacity.



**Figure 3.2:** Hourly electricity production from the modeled North European wind power fleet expressed as a percentage of installed capacity.

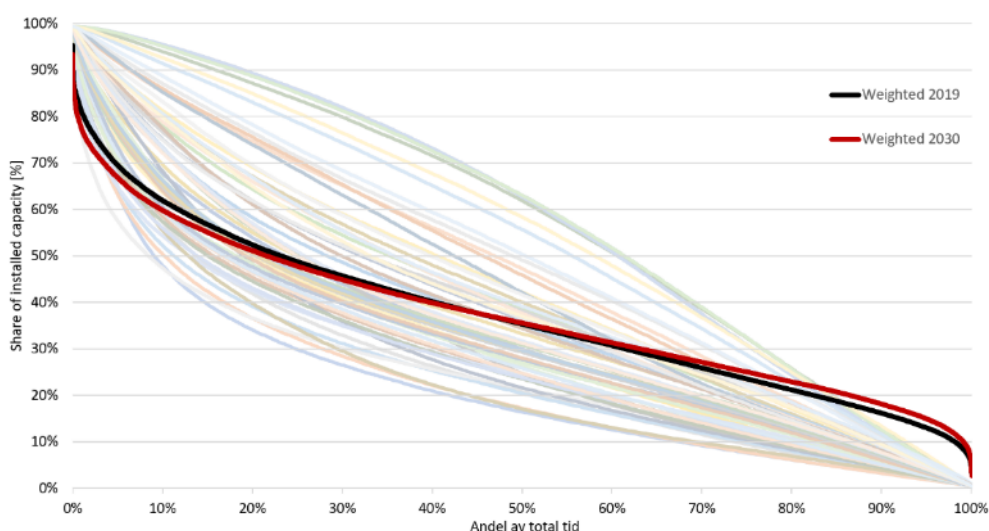


**Figure 3.3:** Duration of wind power production for each analysed location, as a percentage of installed capacity, seen over 2010–2020 and the corresponding duration for the entire Northern European production, 2019 and 2030.

To reach a better understanding of how often the periods of (extremely) low or (extremely) high wind power production occurs during the period 2010–2020 we sorted the hourly production in falling order as a duration diagram, see **Fel! Hittar inte referenskölla..** Each wind farm is represented by one of the pale curves illustrating that there are large differences between locations. The area with the highest production is offshore, outside Germany's northwest coast, and the area with the lowest production is in southern Germany. The area with the highest estimated production has nearly 5,100 full-load hours, while the area with the lowest production has approximately 1,900 full-load hours, based on the specified turbine model mentioned earlier. The thick red and black curves show the aggregate production in the whole of Northern Europe, where red illustrates what it looks like with the installed capacity for 2019 and the black line shows what it looks like based on expected installed capacity in 2030.

The combined Northern European wind power production shows a significantly flatter curve than the corresponding curves of the individual locations. There is thus a clear equalizing effect of spreading the turbines over a large area such as Northern Europe. In other words, if the wind supply is low in some places, it is instead higher in other places. Note that the aggregated curves have significantly fewer hours of low electricity production than the best offshore wind region. As the figure show, the electricity production for the aggregated curves is higher than all individual locations up to about 20% of the installed power, which corresponds to about 15% of total time. This is true, despite the annual electricity generation being more than 50% higher for the best location compared to aggregate electricity generation. In addition, there are many locations that have lower production for a significantly higher proportion of the time, see all the curves below the aggregated curves.

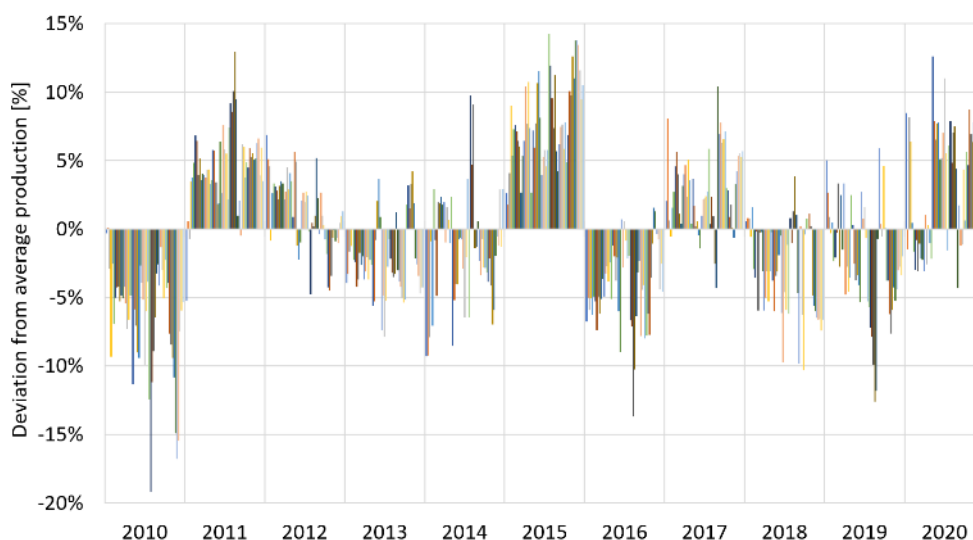


Figure 3.4: Deviation from average annual production for each of the 51 analyzed locations for the period 2010–2020.

It is not only on at short time scale, as one hour, where there is an averaging effect. If we include all 51 analysed locations for northern Europe (Figure 3.1) and compare the annual electricity production there is a quite significant smoothing effect. **Fel! Hittar inte referenskölla.** shows that the annual production varies approximately  $\pm 15\%$  between years for individual wind power areas during the eleven-year period, while this variation is reduced to approximately  $\pm 7\%$  if we aggregate the production for all included locations. This further demonstrates the value of distributing wind farms over a larger area.

Despite the equalizing effects of spreading the wind farms geographically in northern Europe, we still see periods when it is either windy throughout most of the region and periods when the wind potential is low due to low wind speed in much of the region at the same time. We therefore analyzed 3 levels of low electricity production from wind power i.e., sub-10%, 20% and 30% of the total installed capacity for the aggregated fleet. **Fel! Hittar inte referenskölla.** shows the occasions with low production for each of the three levels (10–30%) plotted against the length of each low production period. Note that the x-axis only extends up to 100 hours, while the longest period where the production for sub-30% is 258 hours and for sub-20% is 113 hours. As the figure shows, there are very large differences between the three levels. In addition, it differs a lot between years, as exemplified by the number of occasions when production is below 30% for 20 hours or longer that ranges from 40 to 70 times per year.

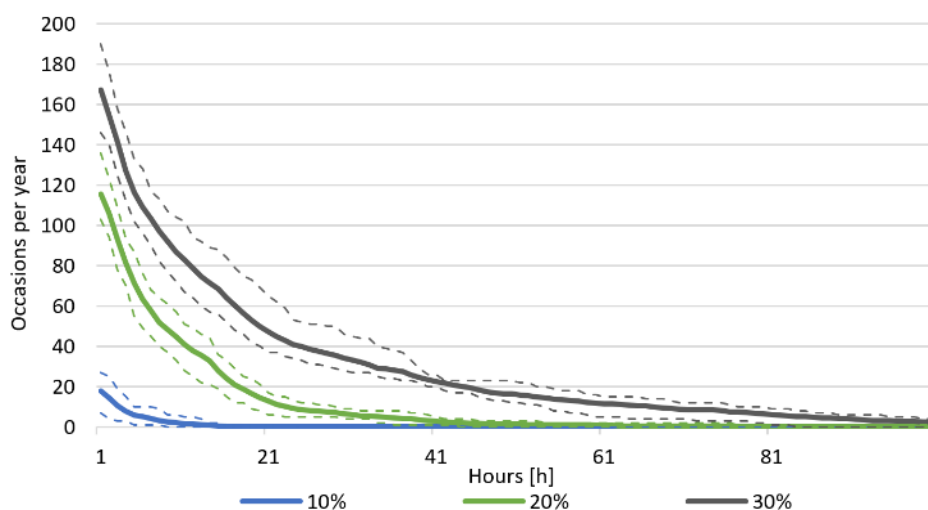
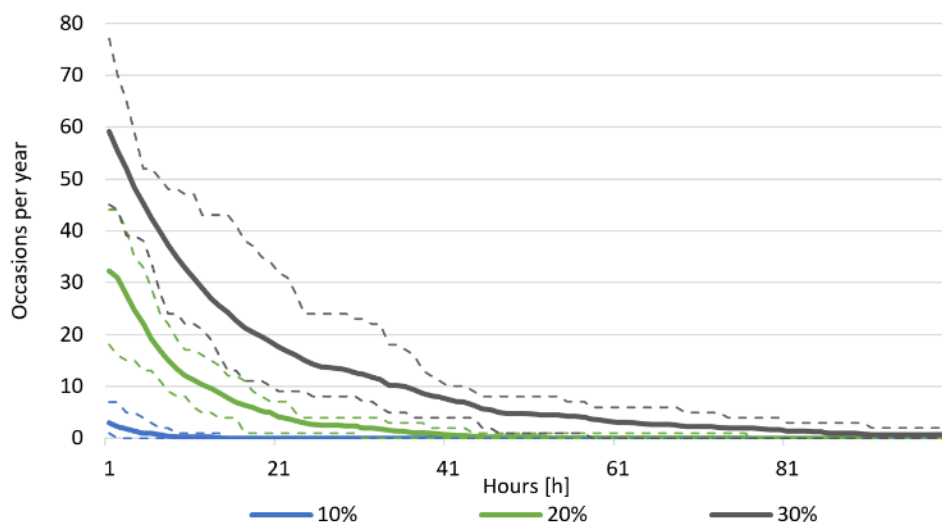


Figure 3.5: Proportion of low wind periods of total time and the length of each period up to 100 hours. The full lines represent the average over the 11-year period and the dashed lines are the corresponding maximum and minimum values.

In **Fel! Hittar inte referenskölla.**, we show the number of occasions when electricity production falls below the three levels (10 – 30%) of total installed power during winter, here defined as October–March. Note that the number of occasions is fewer compared to for the full year (Figure 3.5) as we have removed all low-wind events in the summer half year (April–September). The longest period for which the production is sub-30% is 159 hours (this is the only time it is above 100 hours) and, correspondingly, for sub-20%, 76 hours.



**Figure 3.6: Proportion low production of the winter period and the length of each period up to 100 hours. The full lines represent the average over the 11-year period and the dashed lines are the corresponding maximum and minimum values.**

During the winter half of the year the difference between years is even greater than when including the whole year i.e., the number of occasions with "low production" varies considerably more relative to the average number of occasions. As an example, the occasion when the production is sub-30% for 20 hours or longer ranges between 10 and 34 times per year. In other words, even though there is clearly higher production during the winter compared to the summer, there is a greater variation in the length of periods with low wind during winter compared to summer (or the whole year as the comparison applies). This is something that needs to be considered when developing the electricity system for its use in future climate conditions.

### 3.2 CIRCULATION TYPES

Here, we present results from analysis of historical wind speed conditions stratified following the ten circulation types identified by the SANDRA method. The results, presented as composites are based on the reanalysis-driven HCLIM simulation at 3 km resolution for 1998-2018.

The SANDRA clustering results in distinctly different circulation types (Figure 3.7). The strongest wind speeds over Sweden are associated with westerly to south-westerly flow in situations with low pressure systems to the west or north of Scandinavia (WT1, WT3 and WT6). High-pressure dominated situations (WT2, WT4, WT7, WT8 and WT9) are dominated by low wind speed. Here, we note that the exact location strengths of pressure gradients of the systems determine local differences between the situations. For instance, the situation in WT8 and WT9 differ considerably with the high-pressure system south of Sweden (WT8) and low speed predominantly in the south, while for WT9 the high-pressure system is found to the northeast and in this case higher wind speeds are seen over southern Sweden. It can also be noted that the amplification of wind speed in high-altitude terrain are visible in all maps including also situations with low wind speed (e.g. WT2 and WT4).

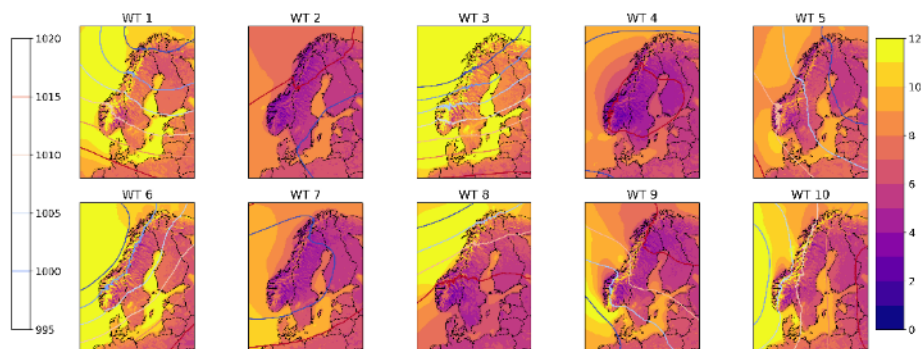


**Figure 3.7:** The ten circulation types (WT1-10) identified by the SANDRA method. Each map shows composite averages for 1998-2018 based on the 3-km reanalysis-driven HCLIM simulation for the respective circulation type of the mean sea level pressure pattern (isolines, unit hPa) and 100-meter wind speed (colours).

Figure 3.18 shows the frequency of the 10 circulation types for each month of the year. Some types (WT2, WT4, WT5 and WT7) peak during the summer months, while others (WT1, WT3, WT6 and WT10) peak during winter. In the figure, we have therefore labelled these as “summer” and “winter” types even if they do occur also in other seasons. For two of the circulation types (WT8 and WT9) peaks are seen in both spring and fall.

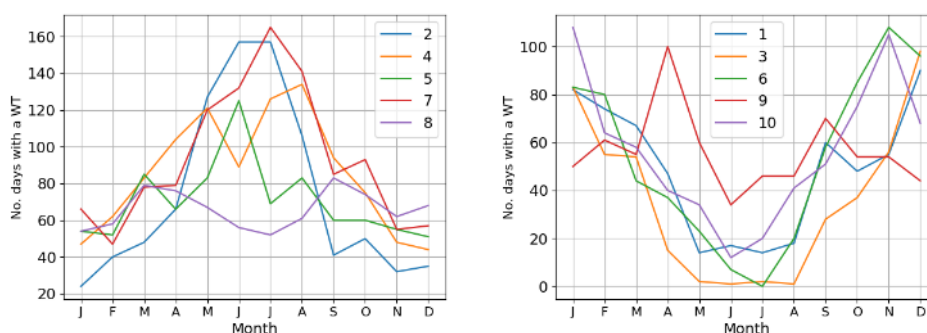


**Figure 3.8:** The frequency of the ten circulation types for each month for 1998-2018. Here, they have been categorized as “summer” (left) and “winter” (right) depending on when they are most frequent.

The number of days with low wind speed is highly dependent on the circulation type. The windy conditions in WT1, WT3 and WT6 (cf. Figure 3.7) are reflected as low frequencies of days with low wind speed in Figure 3.9. Contrastingly, the high-pressure dominated circulation types (WT2, WT4, WT7, WT8 and WT9) stands out with high frequencies of days with low wind speed. Again, as for mean wind speed, geographical details connected to the mountains can be seen in these maps.

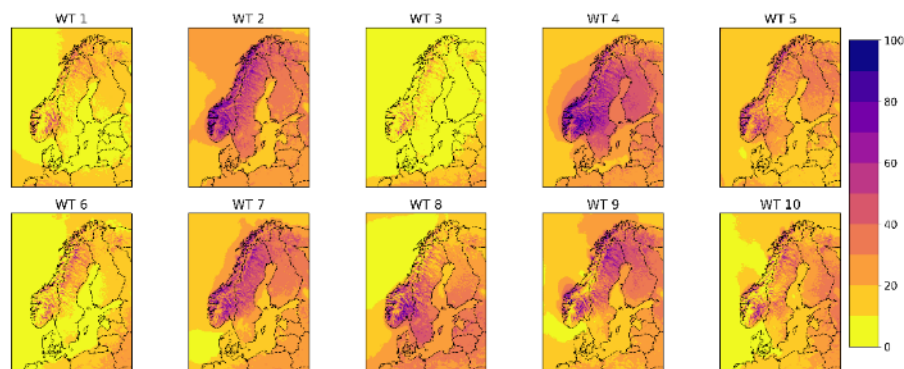


Figure 3.9: Percentage of days with low wind speed (< 4.5 m/s as a daily mean) for each circulation type (WT1-10) in 1998-2018.

Windy conditions favourable of wind power generation (here days with more than 10 m/s in mean wind speed) also show a strong link to the circulation type (Figure 3.10). Again, the low-pressure dominated types show the highest number of days with windy conditions. Geographically, it is clear that the number of days with wind speed above 10 m/s as an average is most common over the ocean. Over land, the mountains stand out as well as some coastal areas and the areas around the large lakes in southern Sweden. The maps show different areas with high numbers in different circulation types. This is a contributing factor to explain the equalizing effect discussed in Chapter 3.1.

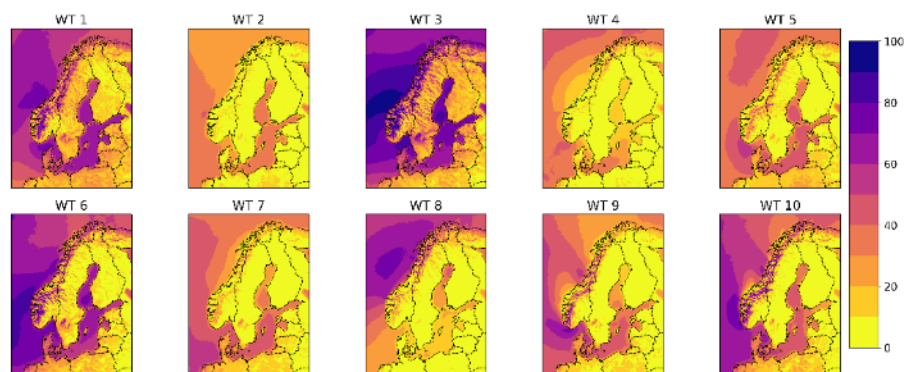


Figure 3.10: Percentage of days with windy conditions (> 10 m/s as a daily mean) for each circulation type (WT1-10) in 1998-2018.

The windiest conditions with wind speed on average above 25 m/s as a diurnal mean are more or less absent for the region (Figure 3.11). It is only in some circulation types occur over parts of the northern Atlantic and in some high-altitude areas along the Swedish mountain range.

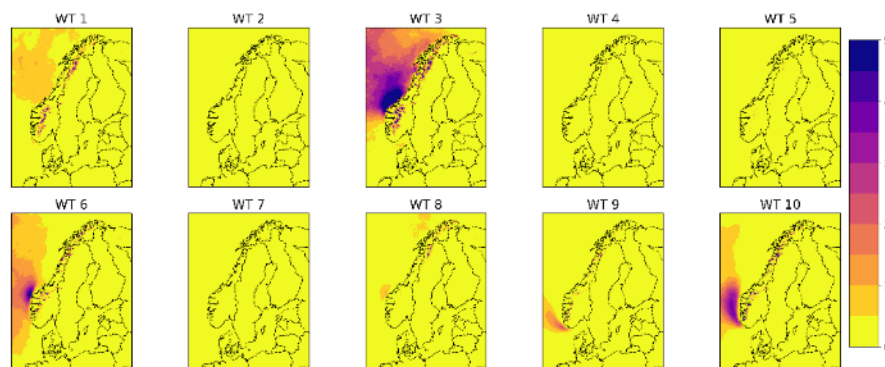


Figure 3.11: Percentage of days with very high wind speed (> 25 m/s as a daily mean) for each circulation type (WT1-10) in 1998-2018.

### 3.3 EVALUATION OF THE REGIONAL CLIMATE MODEL HCLIM

When it comes to validating HCLIM against observations it is not suitable to use straight up correlation between the datasets, since the data from HCLIM is not time-synchronized.<sup>5</sup> In order to evaluate the model, we have instead performed analysis that investigate how well HCLIM describes the characteristics of the wind climate. The intention is primarily to investigate whether there are any systematic deviations between model and observations.

Comparing climatological mean conditions reveals that HCLIM to a strong degree replicates the wind climate as given by ERA5 (Figure 3.12). Deviations include generally lower wind speed over most land areas and higher wind speed in the mountainous part of Scandinavia. Differences can also clearly be seen along the coasts between the two different resolutions with larger deviations in relation to ERA5 at the highest horizontal resolution.

A more detailed comparison for different percentiles of daily mean wind speed at the 161 observational sites in Sweden (Figure 2.1) is shown in Figure 3.13. Here, it is seen that HCLIM at 3 km horizontal resolution clearly outperforms both the coarser 12 km model and ERA5 in the mountainous region where the match between the 3 km model and observations is very good for all quantiles indicative of a strong added value in high-resolution modelling of wind speed in areas of complex terrain. Also, HCLIM shows a general better agreement over land in both HCLIM simulations compared to ERA5 and it is only for low wind speed in the coastal areas where ERA5 show better agreement with observations. Even if the agreement is in general good there are some biases. Most of these indicate that HCLIM at 3 km underestimates wind speed in some situations. For the coastal areas this is both at very low and very high wind speed for all seasons. Also for land areas there is a tendency for underestimating both low and high wind speed in summer while in winter agreement for low wind speed is much better.

<sup>5</sup> HCLIM is a local model that uses data from ERA-Interim at the edge of the analysis area, which is roughly Scandinavia, but within this area there is no temporal coupling.

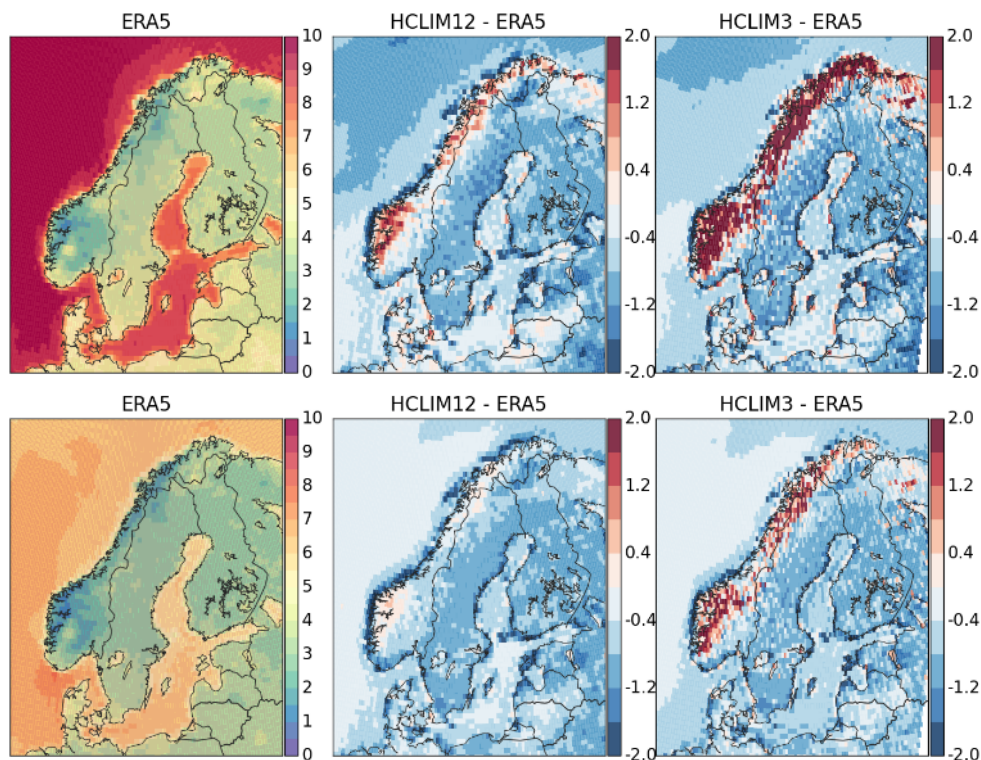


Figure 3.12: Seasonal mean wind speed for winter (DJF, upper) and summer (JJA, lower) in the reanalysis ERA5 (left). Deviations from ERA5 in HCLIM at 12 km (middle) and 3 km (right) horizontal resolution. Both HCLIM simulations have been interpolated to the ERA5 grid before calculating the differences. Unit: (m/s).

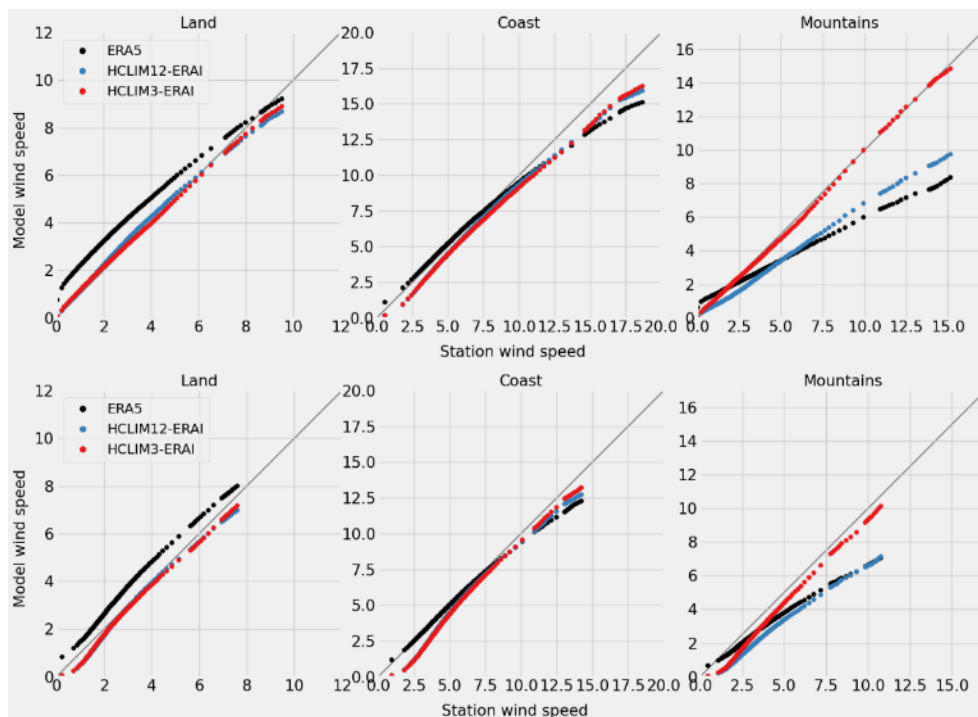


Figure 3.13: Comparison of daily mean wind speed at the 10m level between HCLIM and the 161 observations in three different land categories as outlined in Figure 2.1. Each dot represents one percentile. The upper row represents winter (DJF) and the lower row summer (JJA). Units: (m/s).

Having seen that HCLIM can simulate mean features of the wind climate near the surface in different parts of Sweden we now turn to hub height to evaluate its capability of simulating wind power production potential. We use wind data from all 10 wind farms described in Table 2.1. We focus on SE1.1 for the illustrations in this section while, for the other wind farms, only tabular results are shown to get an idea of the relationship between model results and measurement data.

Table 3.2 shows measured average wind speed for all wind farms, as well as the highest and lowest average wind speed in each wind farm. The table also includes HCLIM average wind speed and hub height for the turbines in each windfarm. On a general level, simulated mean wind speeds are in good agreement with the observations. For half of the wind farms the model is within  $\pm 10\%$  of the observations and for the rest within  $\pm 15\%$ . However, biases do exist. For example, we note that for wind farm SE1.1 the average wind speed is biased low at 5.8 m/s according to HCLIM compared to the observations showing on average 6.5 m/s.

**Table 3.2: Measured and HCLIM average wind speed (m/s) based on 3-hourly data, plus hub height (m) for each wind farm (see Table 2.1 for details).**

Average wind speed	SE1.1	SE1.3	SE1.4	SE2.1	SE3.1	SE3.2	SE4.1	SE4.2	SE4.3	SE4.4
Obs. average	6.5	7.0	7.3	7.0	6.7	6.3	6.2	6.2	6.3	5.9
Obs. Max	6.9	7.3	7.3	7.8	7.5	6.8	6.4	6.5	6.6	6.2
Obs. Min	6.2	6.7	7.3	6.2	6.5	6.1	5.8	6.0	6.0	5.7
HCLIM average	5.8	6.0	7.3	6.5	6.6	7.1	6.5	6.8	6.5	6.5
Hub height	120	105	100	95	119	100	90	80	90	90

An explanation for the underestimation at SE1.1 could potentially be differences in height with the actual hub height at 120 meters while the HCLIM data represents the 100-meter level. However, when looking at all 10 wind farms there is no clear systematic deviation in mean wind speed compared to measured values in relation to differences between actual hub height and the 100-meter level. It can also not be excluded that differences in local conditions play a role for the differences between observations and HCLIM in Table 3.2. As the table show there can be quite large differences between the highest and lowest average wind speeds observed in the area of a wind farm. Here, HCLIM data is selected for an area judged to be representative of the wind farm, while the measured data is a median<sup>6</sup> for all turbines in the wind farm for which data was available. This means that the areas do not overlap completely. Despite the relatively high spatial resolution in the climate model (3x3 km), small-scale differences in the landscape are not resolved by the model, which can have a large impact on local wind speed.

To get a more in-depth picture of differences between observations and HCLIM, Figure 3.14 shows the wind speed distributions for wind farm SE1.1 during the entire analysis period. As can be seen, they generally overlap well, with the main difference being that the observations have a higher proportion of instances with wind speeds above 10 m/s. At levels above 15 m/s, HCLIM data is more or less

<sup>6</sup> The reason for using median values is that there are various deficiencies in data quality (e.g. missing data or frozen values) where median values have been deemed the best way to handle this. In cases where the data quality generally was too low for the wind farm, this has excluded the analysis.

completely missing for this specific example. This may partly be a consequence of the wind turbines here having a higher hub height than the HCLIM data. We also point to the similar tendency, of underestimating high wind speeds, as illustrated above for the 10-meter level. Another potential explanation for the disagreement between HCLIM and observations could be that pointwise measurement data varies more than gridded model results.

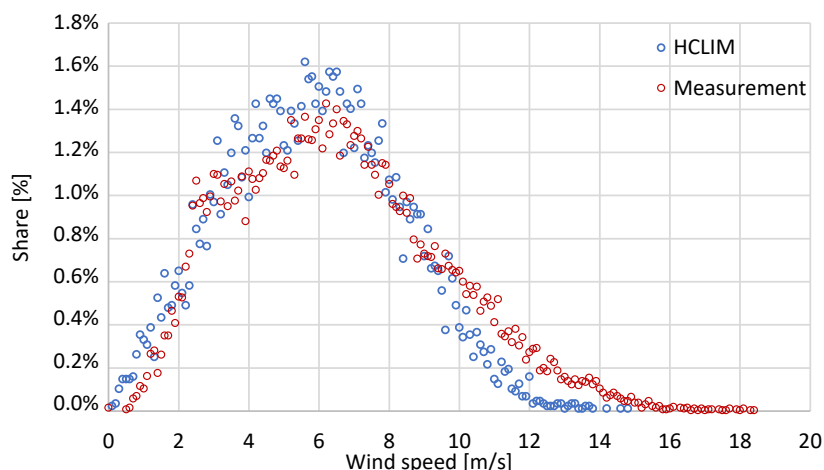


Figure 3.14: Wind speed distribution for measured data in wind farm SE1.1 and the HCLIM-model for 2016–2018.

We have also compared how the wind is distributed over the months of the year and here too there is a relatively good agreement between model data and measurement data, see Figure 3.15. HCLIM underestimates wind speed throughout the year with largest differences during the summer (April–September). However, compared to the observations, HCLIM shows a slightly greater difference between summer and winter.

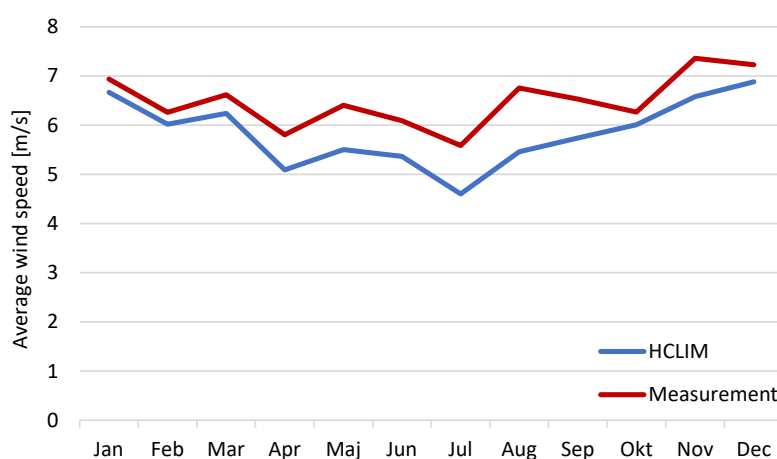


Figure 3.15: Average wind speed per month for measurements in wind farm SE1.1 and HCLIM data.

Also at the other individual wind farms it is found that the HCLIM captures the seasonal pattern well, see Table 3.3. The correlation between observed and simulated monthly averages is high for most of the wind farms, but somewhat lower for SE1.1 due to the bias in the seasonal cycle as discussed above. However,

the results for the other wind farm differs and there is no evidence of any systematic difference between summer and winter in HCLIM compared to the observations.

**Table 3.3: Correlation between observed and simulated monthly average wind speed for each wind farm. Mean wind speed for the winter half year (October-March) and summer half year (April-September) are also given.**

Monthly average	SE1.1	SE1.3	SE1.4	SE2.1	SE3.1	SE3.2	SE4.1	SE4.2	SE4.3	SE4.4
Correlation	0.82	0.92	0.87	0.93	0.96	0.94	0.94	0.92	0.78	0.82
HCLIM winter [m/s]	6.4	6.6	8.3	7.2	7.5	7.4	7.1	7.3	7.1	7.1
HCLIM summer [m/s]	5.3	5.4	6.3	5.8	5.8	6.4	6.0	6.2	6.0	6.0
Difference [m/s]	1.1	1.2	2	1.4	1.7	1	1.1	1.1	1.1	1.1
Obs. winter [m/s]	6.8	7.8	8.1	7.6	7.8	7.0	6.6	6.7	6.8	6.4
Obs. summer [m/s]	6.2	6.3	6.5	6.3	5.8	5.5	5.7	5.7	5.9	5.6
Difference [m/s]	0.6	1.5	1.6	1.3	2	1.5	0.9	1	0.9	0.8

We also investigate how the wind speed varies over the day, Figure 3.16. Here, we have divided the comparison into the winter half year (October-March) and the summer half year (April-September) to identify if there are any systematic differences. As the figure shows the average wind speed at hub height is slightly higher in the evening and night (18–03) compared to the day (06–15), both for measured data and HCLIM. There are relatively small differences between winter and summer. For SE1.1, that is shown in the figure, there is a slightly greater difference between winter and summer in HCLIM compared to the measurement data.

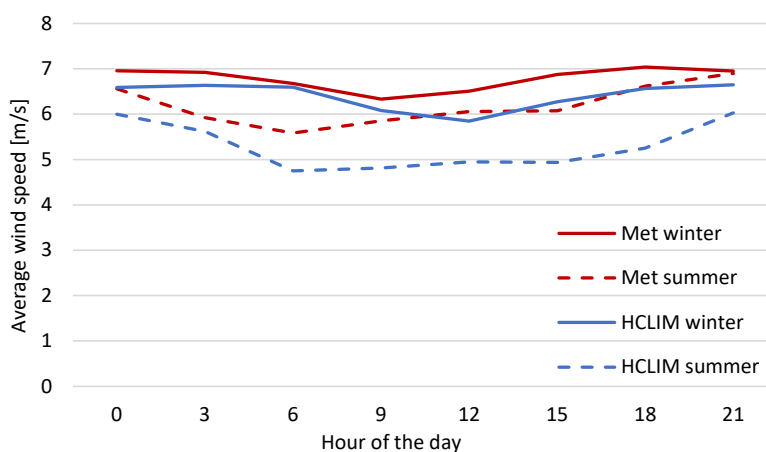


**Figure 3.16: Average wind speed for every third hour for wind farm SE1.1 and HCLIM for summer and winter.**

Table 3.4 shows the difference in average wind speed between night and day for all wind farms, where a positive value means that the wind speed is higher during the night compared to the day. Similar to SE1.1, both observations and HCLIM indicates that wind speed is generally higher during night than during day. This relationship is more evident in summer, while the difference between night and day is smaller in winter. In general, there is a systematic deviation between HCLIM and observations with HCLIM generally overestimating the difference between day and night compared to the observations.

**Table 3.4: Difference in average wind speed between night (average over data from 18, 21, 00, 03) and day (06, 09, 12, 15) for observations and HCLIM.**

Daily variation	SE1.1	SE1.3	SE1.4	SE2.1	SE3.1	SE3.2	SE4.1	SE4.2	SE4.3	SE4.4
HCLIM winter [m/s]	0.41	0.39	0.42	0.37	0.59	0.49	0.38	0.31	0.38	0.38
Obs. winter [m/s]	0.37	0.30	0.22	0.16	0.37	0.28	0.10	-0.05	0.26	0.3
Diff. winter [m/s]	0.04	0.09	0.20	0.21	0.22	0.21	0.28	0.36	0.12	0.08
HCLIM summer [m/s]	0.86	0.86	1.05	0.84	0.93	0.88	0.43	0.34	0.43	0.43
Obs. summer [m/s]	0.61	0.78	0.59	0.64	0.54	0.87	0.01	-0.47	0.45	0.46
Diff. summer [m/s]	0.25	0.08	0.46	0.20	0.39	0.01	0.42	0.81	-0.02	-0.03

Stronger night-time wind speeds are seen for all assessed parks except one, SE4.2, for which daytime wind speed is higher. HCLIM also shows a smaller, albeit still positive, difference between night and day for this particular location. This wind farm is located very close to the coast, which means that differences between day and night could potentially be influenced by sea-land breeze circulations, especially in spring and early summer. Despite relatively high spatial resolution in the model, the description of a small-scale phenomenon such as sea breeze is not complete, and it is not expected that HCLIM will capture this in detail.

Next, we investigate how HCLIM represents conditions with low wind speed as this is an important aspect for the energy system. Table 3.5 shows the temporal correlation between months between HCLIM and the observations for the proportion of occasions with low wind speed. Here, low wind speed is defined by occasions with wind speed less than three different wind speed levels. As can be seen from Table 3.5, the correlation is high, i.e. the share of low wind speed occasions simulated by HCLIM follows the observed one on a monthly basis. However, for a few wind farms, the correlation drops notably at the lower limit value (4.5 m/s). This shows that there is a sensitivity to threshold values in the analysis where different data sets are compared to each other and is an important relationship to include in future studies of wind speed.

**Table 3.5: The correlation between HCLIM and measured data regarding low wind on monthly basis.**

Wind limit	SE1.1	SE1.3	SE1.4	SE2.1	SE3.1	SE3.2	SE4.1	SE4.2	SE4.3	SE4.4
< 4.5 m/s	0.63	0.98	0.86	0.98	0.97	0.96	0.84	0.73	0.83	0.60
< 5.5 m/s	0.78	0.98	0.90	0.98	0.97	0.96	0.89	0.87	0.91	0.90
< 6.5 m/s	0.81	0.98	0.94	0.98	0.97	0.96	0.86	0.89	0.95	0.87

For high wind speeds, which also are of interest, we can state that observations from the turbines have a higher proportion of occasions with wind over 15 m/s compared to HCLIM for most wind farms, see Table 3.6. This is partly linked to the fact that the average wind speed differs between observations and HCLIM. Other reasons may involve observations tending to vary somewhat more compared to HCLIM or that there are relatively large differences in wind conditions between the wind turbines within a wind farm. Local factors involving dependency on location in the terrain and the wake effects that occur between the wind power in different wind directions may also play a role. Note that apparent differences in the fraction of occasions with high wind speed between the wind farms may be a result not analysing identical years due to data availability.

**Table 3.6: Frequency (in %) of wind speed over 15 m/s for HCLIM at three hourly resolution and from the observations for three respectively one-hourly resolution.**

Wind limit	SE1.1	SE1.3	SE1.4	SE2.1	SE3.1	SE3.2	SE4.1	SE4.2	SE4.3	SE4.4
HCLIM 3-h	0.00%	0.10%	1.67%	0.34%	0.72%	0.52%	0.71%	0.59%	0.15%	0.10%
Obs. 3-h	0.32%	0.68%	1.93%	1.02%	0.65%	0.50%	0.27%	0.77%	0.28%	0.08%
Obs. 1-h	0.42%	0.77%	2.28%	1.34%	0.79%	0.57%	0.31%	1.06%	0.34%	0.12%

The table also shows that the proportion of occasions when the wind exceeds 15 m/s increases slightly at a higher time resolution, i.e. at 1-hour average values. We also checked what happens with an even higher resolution, in the cases we had access to 10-minute averages. In those cases (not shown), the proportion increases by approximately 0.1% compared to 1-hour averages.

We also looked at the proportion of very high wind speeds, for example above 20 m/s. Such, more extreme wind speeds are rare in their nature and for SE1.1 it never occurred during the analysed three-year period. In the seven-year record for SE3.2, with generally higher wind speed, it occurred 0.03% of the time (and only during one of the almost seven years).

### 3.4 CHANGES IN THE WIND CLIMATE IN HCLIM

Here, we focus on how the simulated wind climate in the high-resolution HCLIM model changes as a result of continued global warming. Results shown are focussing on the very strong forcing scenario RCP8.5 at the end of the century. Before describing potential changes for the wind power production, we first look at the 10-meter level to illustrate how changes may differ due to different resolution in the models.

#### *Changes in near surface wind speed*

Figure 3.17 shows wintertime wind speed as simulated by HCLIM at 12 and at 3 km horizontal resolution when driven by the two global models EC-Earth and GFDL (see details in Ch. 2.2). Similar to the ERA-Interim driven simulations assessed in Ch. 3.2, we note that also here, for the GCM-driven simulations, there are differences in details between the 12- and 3-km model versions. The same applies for summer as seen in Figure 3.18. For both seasons higher wind speeds over the ocean than over land is the most prominent difference. There are also strong contrasts over land with high wind speed in high-altitude exposed areas and some coastal areas and low wind speed in low-altitude areas leeward of the mountains. Comparing the two GCM-driven simulations, we note that most regional features in the wind climate are relatively similar. However, there are some exceptions with higher average wind speed both in winter and summer in the GFDL-driven simulations compared to the EC-Earth-driven ones over part of the northern Atlantic Ocean.

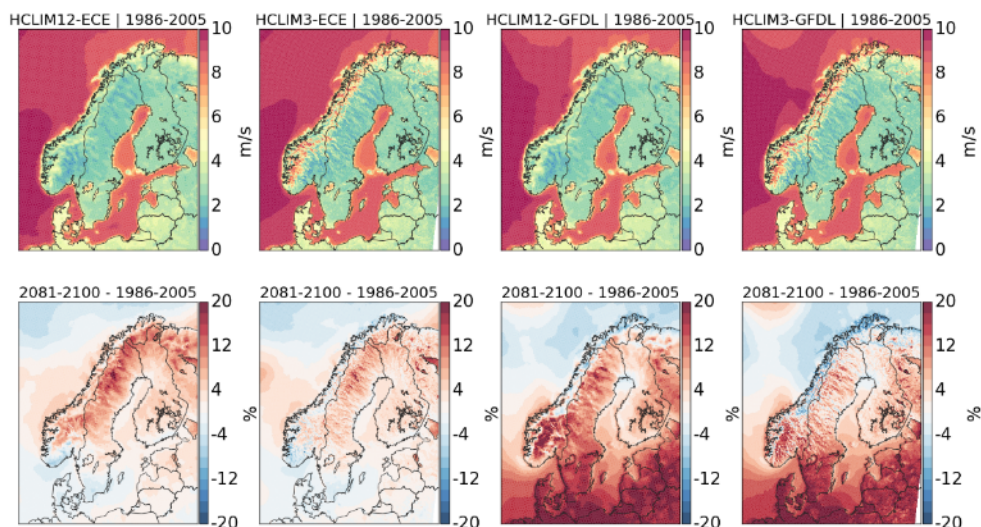


**Figure 3.17:** Average wind speed at the 10-meter level for the historical period (upper row) as simulated by HCLIM at 12 respectively 3 km horizontal resolution for winter (DJF). The panels to the left shows EC-Earth (ECE) driven simulations while the panels to the right shows the GFDL-driven ones. The lower row shows relative changes (in %) from 1986-2005 to 2081-2100 in the RCP8.5-driven simulations.

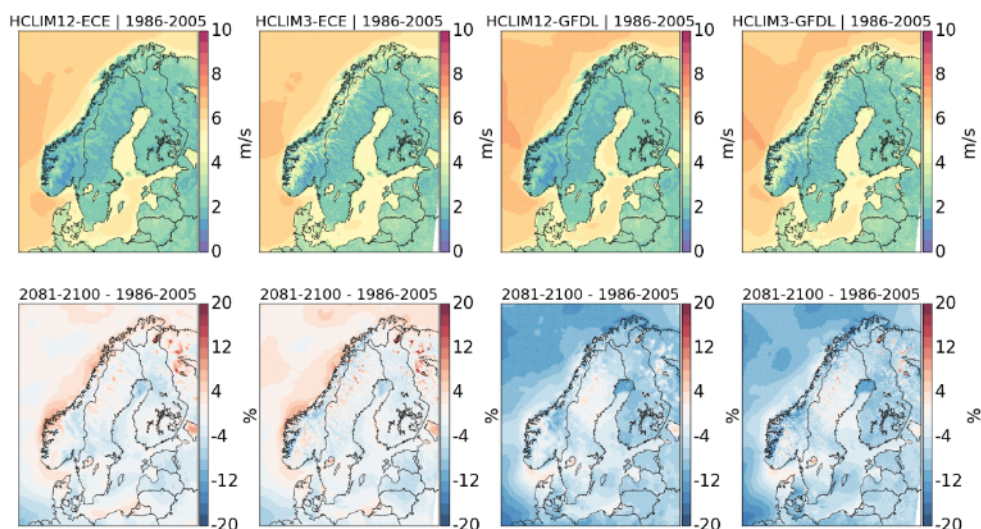


**Figure 3.18:** Average wind speed at the 10-meter level for the historical period (upper row) as simulated by HCLIM at 12 respectively 3 km horizontal resolution for summer (JJA). The panels to the left shows EC-Earth (ECE) driven simulations while the panels to the right shows the GFDL-driven ones. The lower row shows relative changes (in %) from 1986-2005 to 2081-2100 in the RCP8.5-driven simulations.

Both figures (3.17 and 3.18) indicate strong climate change signals in the scenario. It is also clear that there are strong differences depending on which of the global models that is assessed. In general, the 12- and 3-km model versions show climate change signals with both regional patterns and amplitudes being very similar. There are, however, exceptions, for winter the increases in wind speed over land in large parts of the region are stronger in the 12-km version while changes over the ocean are very similar. It is also clear that the 3-km version show more spatial structures to the wind speed changes in large parts of Scandinavia, both in the

mountainous areas and in northern Sweden following structures in the landscape such as river basins in Sweden.

For the 100-meter level we only have model data available from the 3-km version of HCLIM. As at the 10-meter level the simulated seasonal mean wind climate at hub height is highly influenced by the surface conditions (Figure 3.19). Large-scale differences between ocean and land are evident as well as are differences between more exposed locations in high-altitude areas, e.g. western parts of the mountains, and low-lying areas in areas on the leeward side. Also, the climate change signals follow to large extent those at the 10-meter level (cf. Figure 3.17 and 3.18). This includes also small-scale spatial structures indicating strong influence from the surface.

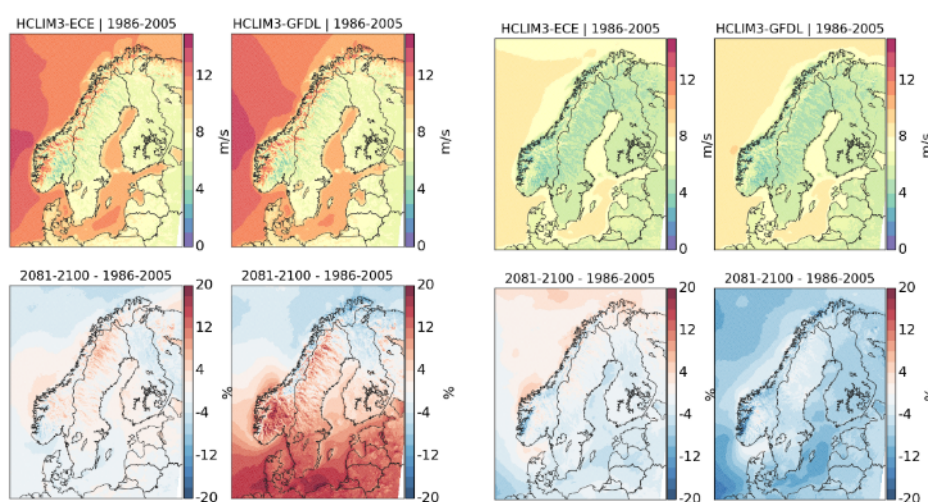


**Figure 3.19:** Average wind speed at the 100-meter level for the historical period (upper row) as simulated by HCLIM at 3 km horizontal resolution for December-February (left) and June-August (right). The left-most panels in each pair shows EC-Earth (ECE) driven simulations while the panels to the right shows the GFDL-driven ones. The lower row shows relative changes (in %) from 1986-2005 to 2081-2100 in the RCP8.5-driven simulations.

#### *Changes in wind power density*

Figure 3.20 shows the annual average wind power density (WPD) in the historical and future simulations, and the differences between them, where HCLIM has been driven by the two different GCMs. All four maps to the left (historical and future conditions) show generally the same pattern and similar WPD in the region. The highest potential is over sea, notably in some areas west of Norway, while the lowest WPD are found over northern land areas in lee of the mountains in Sweden and Finland. In Swedish land areas, there is a gradient with the highest WPD in the south and the lowest ones in the interior of the north. High altitude areas and lakes show relatively high WPD compared to its surroundings.

As for the seasonal maps showing changes in wind speed above (Figure 3.17 and 3.18) there are strong differences in how the WPD changes in the future depending on which of the two global models that are used. Here, the EC-Earth driven simulation shows relatively small changes while there are strong increases the GFDL-driven one.

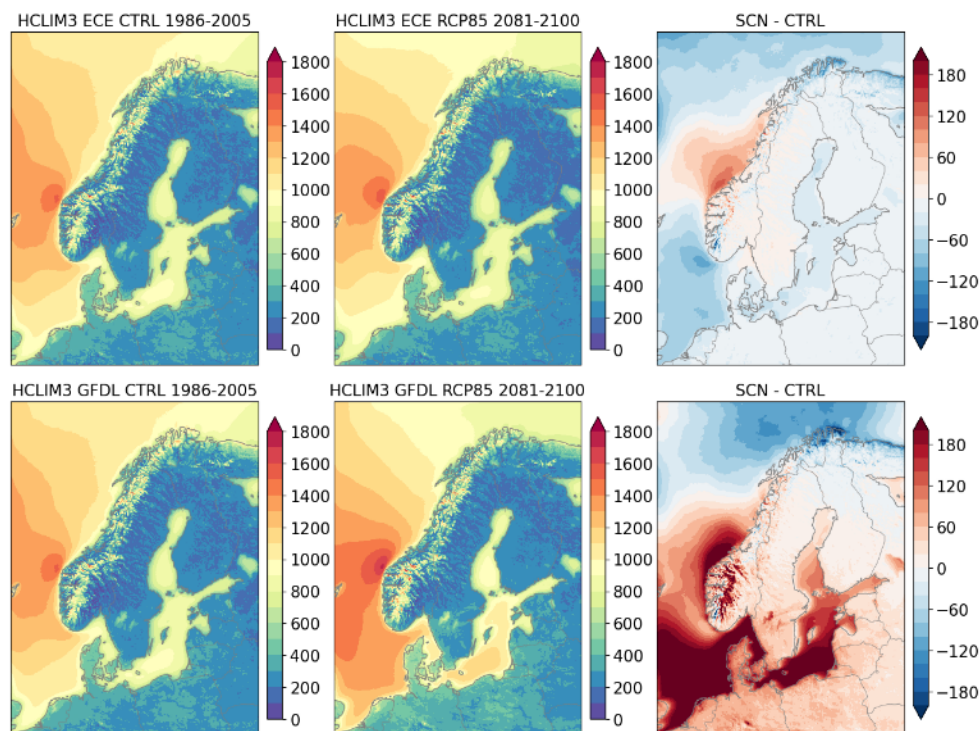


Figure 3.20: Average wind power density at the 100-meter level as simulated by HCLIM at 3 km horizontal resolution for annual mean conditions for: the historical period (left), 2081-2100 under the RCP8.5 scenario (middle) and the difference between scenario and historical period (right). The upper row shows results with boundary conditions from EC-Earth (ECE) while the lower row shows those driven by GFDL. Unit:  $W/m^2$ .

The box-plots in Figure 3.21 summarizes the situation for the four pricing areas in Sweden divided per season and its gradual change over the century in the strongest RCP8.5 scenario. The strong seasonal cycle is reflected in the high numbers in winter (DJF) compared to summer (JJA), with spring (MAM) and fall (SON) in between. The figure also illustrates that wind power has the largest potential in the south for all seasons and time periods. On average, for all seasons and all time periods, WPD in SE4 is around 40% higher than in SE2 and SE3. SE1 also shows higher numbers, by almost 10%, compared to SE2 and SE3, a result from including a high number of high-altitude windy locations in the mountains in the spatial averaging. The spread between different years, as illustrated by the box-whisker diagrams, show strong interannual variability with, for some seasons and regions, differences of about a factor of two in WPD.

For the future, it is clear that the changes with time in the two simulations show different features for the two models in different seasons and pricing areas. For example, the strong increase in WPD in southern Sweden in the GFDL-driven simulation seen in the annual mean (Figure 3.20) is mainly confined to winter, while the same simulation shows decreases in summer. Averaging over the whole year, the EC-Earth-driven simulation shows small (up to  $\pm 3\%$ ) changes for all four pricing areas. The GFDL-driven simulation shows up to  $\pm 4\%$  in SE1 and SE2, while increases in SE3 and SE4 are about 7% in the mid-century and 14% in the late-century period. For some seasons, however, differences can be larger. The GFDL-

driven simulation yields both the maximum relative increase (23% in SE4 for summer) and maximum decrease (-36% in SE4 for winter).



**Figure 3.21:** Wind power density at the 100-meter level as simulated by HCLIM at 3 km horizontal resolution for the four seasons and averaged over the four electricity price areas in Sweden (see Figure 2.1). All numbers are from the RCP8.5 scenario where HCLIM has been taking boundary conditions from EC-Earth and GFDL respectively. Shown are median (solid line inside the box), 25<sup>th</sup> and 75<sup>th</sup> percentiles (box) and 5<sup>th</sup> and 95<sup>th</sup> percentiles (whiskers) representing the interannual variability. Abbreviations in the legend relates to: CTRL (the historical period 1986-2005), Mid-C (mid-century 2041-2060), End-C (end of century 2081-2100). Unit: W/m<sup>2</sup>.

### *Changes in days with low wind speed*

Figure 3.22 shows that days with low wind speed (less than 4.5 ms<sup>-1</sup> as a diurnal mean) in winter generally are most common in regions in the mountain chain with exception to the highest most central parts where there is a local maximum. Local maxima are also seen in Sweden east of the mountains following the terrain. Areas with absolute minima are seen over the sea, most pronounced over the North Atlantic but also over the Baltic Sea. As for WPD there is a strong similarity between the general patterns in all four panels to the left indicating that these features, that to a strong degree are forced by the topography, are robust. However, there are also differences between them reflecting climatological differences over 20-year periods.

The climate change signal, shown to the right, differs radically between the two simulations with the EC-Earth-driven simulation indicating more days with low wind speed over relatively large parts of southern land areas, while the GFDL-driven simulation on average show decreasing number of days with low wind speed over most of the domain. Both simulations agree on increased number of days with low wind speed in the far north. A common pattern for the two is that areas downwind of the highest mountains, both in Sweden and Norway, are projected to have less days with low wind speed in the future. As this pattern appear to be governed by the local and regional details of the orography they may be related to surface processes. A potential mechanism could involve reduced snow on the ground leading to higher near-surface temperatures, which would reduce the potential to form strong high-reaching inversions in valleys.

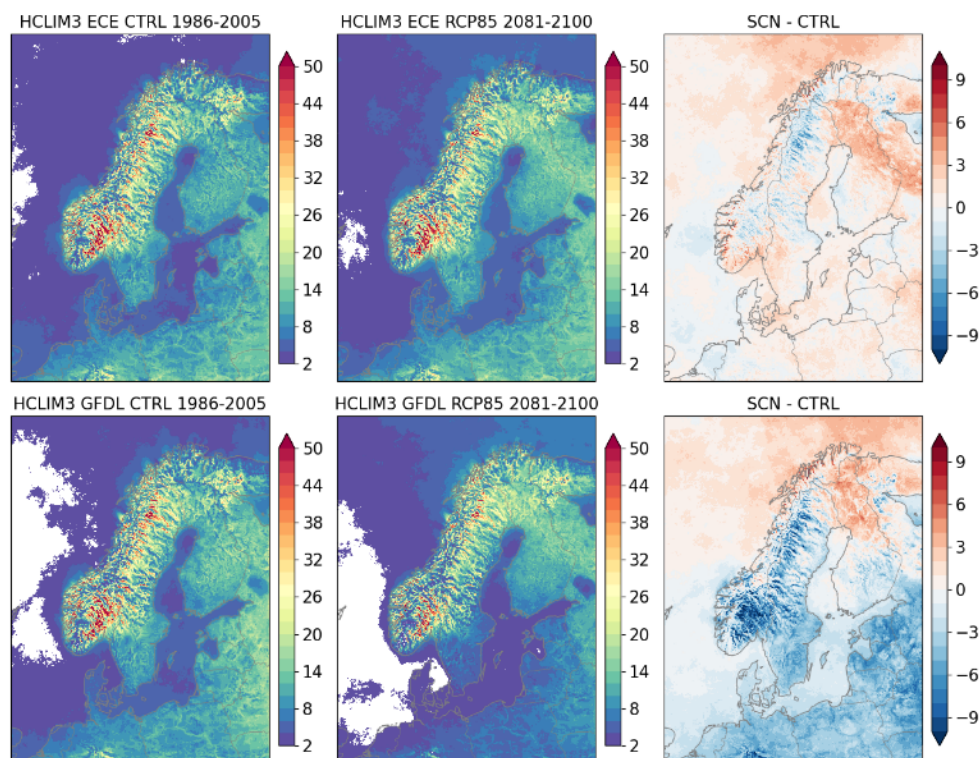


Figure 3.22: As Figure 3.20 but for the frequency of days with low wind speed (less than  $4.5 \text{ m s}^{-1}$  as a diurnal mean) at the 100-meter level in winter (DJF). Unit: days/year.

In summer there is an extended maximum of days with low wind speed over large parts of Scandinavia (Figure 3.23). Again, with exceptions in parts of the highest central parts of the mountains. In other regions there are strong contrasts between sea (and lakes) and land. The four maps indicate some differences both in time between scenario and historical period and between the two experiments with GFDL and EC-Earth. As for winter, the climate change signal differs significantly between the two simulations with the GFDL-driven simulation indicating a larger increase in the number of days with low wind speed over most areas, whereas the EC-Earth-driven one also show increases in the south but decreases in the far north. We also note some orographically induced structure to the climate change signal in some areas close to the mountains. Potentially, this could be related to changes in temperature conditions and vertical stability as discussed for winter above. Compared to winter, however, both areas and amplitudes are smaller.

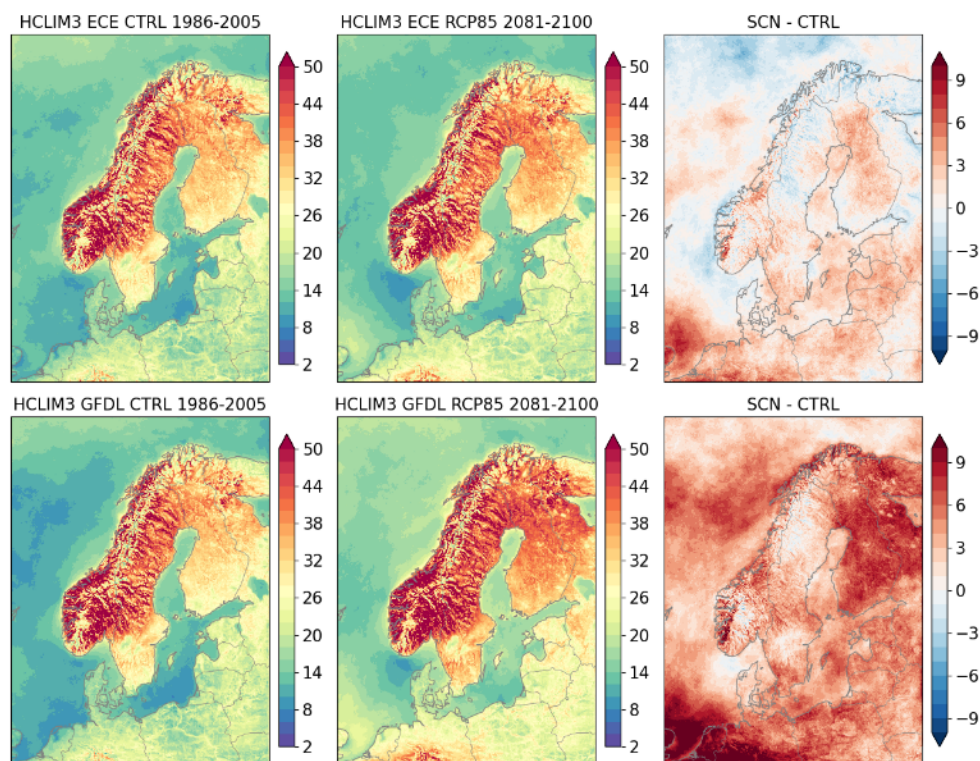


Figure 3.23: As for Figure 3.20 but for the frequency of days with low wind speed (less than  $4.5 \text{ m s}^{-1}$  as a diurnal mean) at the 100-meter level in summer (JJA). Unit: days/year.

#### *Changes in days with full load hours*

Figure 3.24 and 3.25 show that the simulated number of full load hours (more than  $10 \text{ m/s}$ ) are strongly dependent on the geographical location with maxima over ocean areas. For winter, the maps indicate more than 1200 hours per year west of Scandinavia, corresponding to more than half of the time<sup>7</sup>. Even for summer there are high numbers in this region, corresponding to about 30% of the time. Over land, there is a general gradient with high numbers in the south and low numbers in the north and in the east. In addition, lakes and coastal areas have relatively many full load hours as does high-altitude mountain areas. Lower numbers over land are seen leeward of the mountains. In winter, large parts of northern Sweden show a complex pattern of maxima and minima to a large extent following terrain. This pattern is not seen in summer.

The climate change signals, indicate small changes over the ocean for winter. Over land, there are strong differences between the GFDL-driven simulation, showing increases of full load hours over most land areas except for the most northern parts, and the EC-Earth-driven one showing relatively small changes. As for low-wind days, there is an imprint of the orography on the climate change signal with differences between high and low altitude locations.

<sup>7</sup> Total number of hours in winter (DJF) is 2160 (90 days times 24 hours).

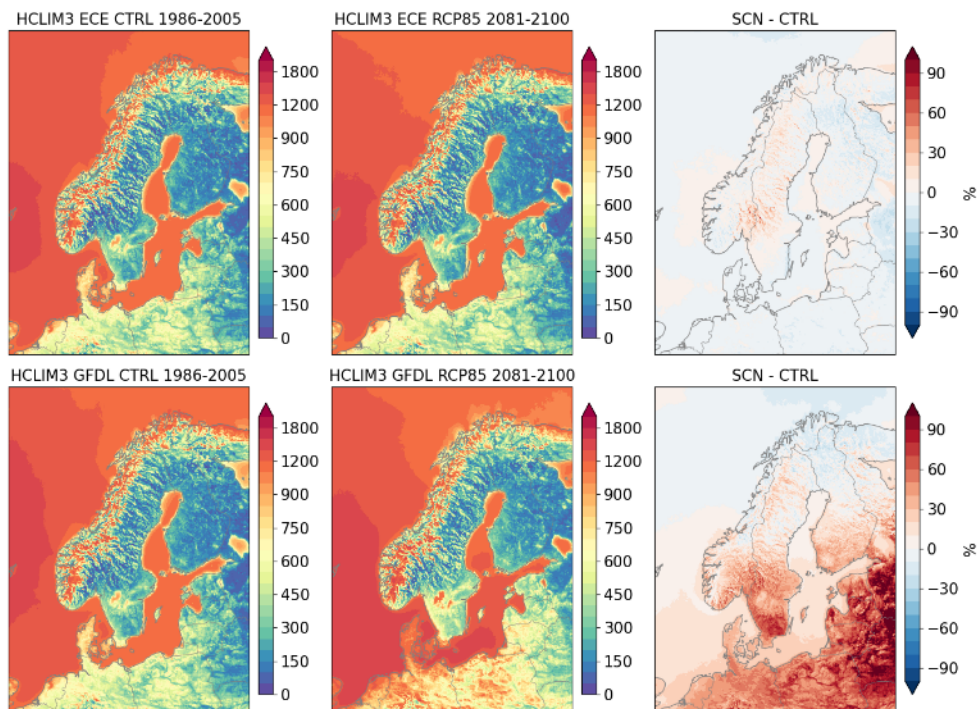


Figure 3.24: As Figure 3.20 but for full load hours (FLD, here more than  $10 \text{ ms}^{-1}$ ) at the 100-meter level for winter (DJF). Unit: hours/year.

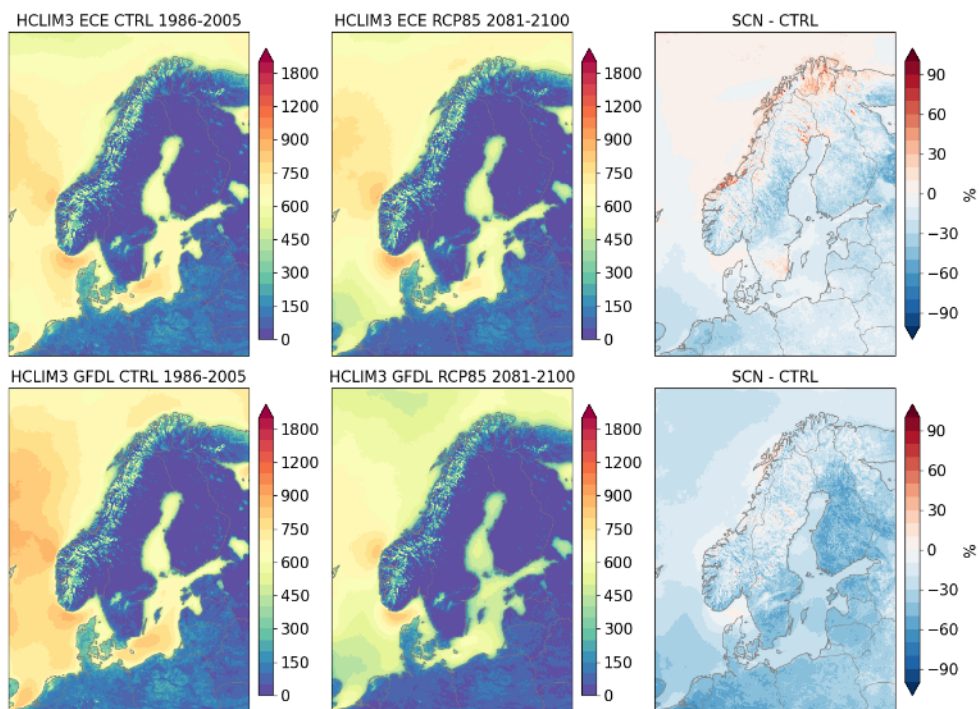


Figure 3.25: As Figure 3.20 but for full load hours (FLD, here more than  $10 \text{ ms}^{-1}$ ) at the 100-meter level for summer (JJA). Unit: hours/year.

For summer, both simulations indicate decreasing number of full load hours over the North Sea and the Baltic Sea. In the GFDL-driven simulation the number of full load hours decreases also over other parts of the North Atlantic. Both simulations indicate decreasing number of full load hours over almost all land areas with some exceptions in the EC-Earth-driven simulations.

*Changes in very high wind speed*

Figure 3.26 shows that occasions with very high wind speed (more than 25 m/s) generally are absent over most land areas. Exceptions are high-altitude areas in the mountains and areas along the North Sea and Baltic Sea coastlines including much of Denmark and the Swedish west and south coasts. As for WPD and days with low wind speed these features are robust and to a strong degree governed by the topography, but again, with differences reflecting changes or variability in the climate.

The climate change signal, shown to the right, differs radically between the two simulations with the GFDL-driven simulation on average showing a strong increase of days with very high wind speed over the North Sea and large parts of the Baltic Sea. For the northern half of the domain changes are more similar, still with some differences.

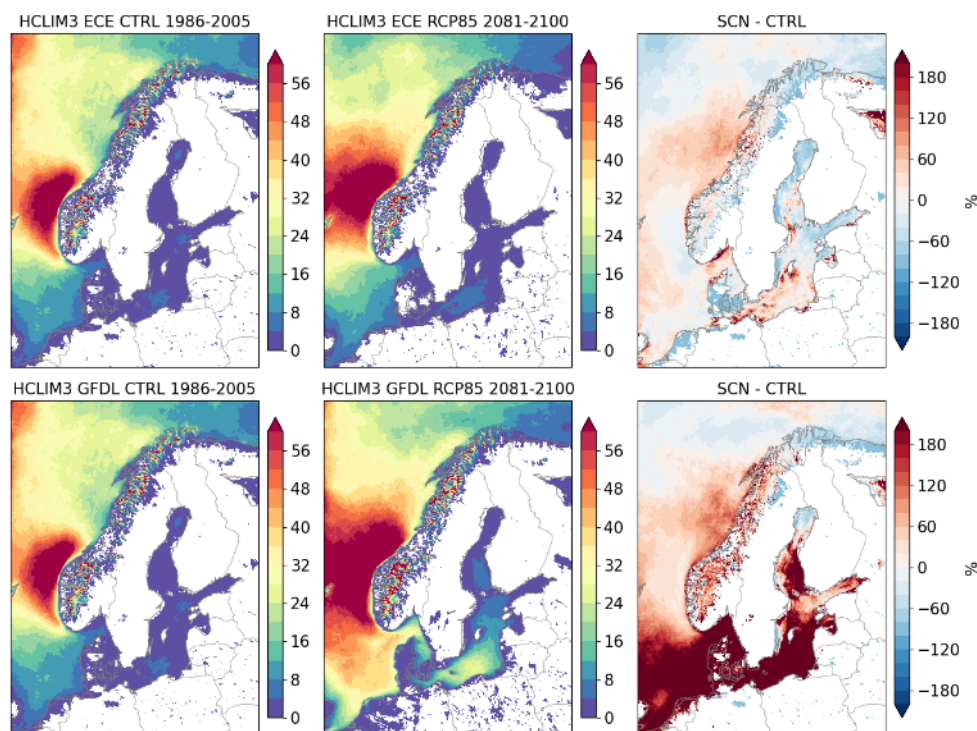


Figure 3.26: As Figure 3.20 but for the frequency of hours with very high wind speed (more than 25 ms<sup>-1</sup>) at the 100-meter level. Units: hours/year and %.

### 3.5 CHANGES IN ICING CONDITIONS IN HCLIM

As icing of wind turbines and other relevant infrastructure may pose a problem to wind power generation we investigate to what degree icing conditions may change in the future. A simple index, considering high liquid cloud water content in situations with temperatures below the freezing point, is applied on the high-resolution HCLIM simulations for the 100-meter level.

As the absolute number of days with risk of icing are sensitive to the cloud microphysics (Kringelebotn Nygaard et al. 2011), and as we have no detailed observations of the relevant variables, we have not done any model evaluation for risk of icing. Bearing in mind that the numbers should be taken as a crude indicator we note that wintertime (DJF) conditions reveals a clear temperature influence from the sea (Figure 3.27). On average, there are very few hours per year with risk of icing in all coastal areas also in the north. The number of hours is generally higher in the northern and eastern parts of the domain. The Scandinavian mountain region show a complex pattern with generally high number of hours in interior and high-altitude areas and low number of hours in coastal regions.

The climate change signals seen in the right part of the figure indicate decreasing risk of icing condition in more or less all areas in the south and also along the coasts of the Gulf of Bothnia. Contrastingly, interior parts of the mountain chain and northern parts of Sweden show increasing risk. This is also found for northern Finland, Norway, and Russia.

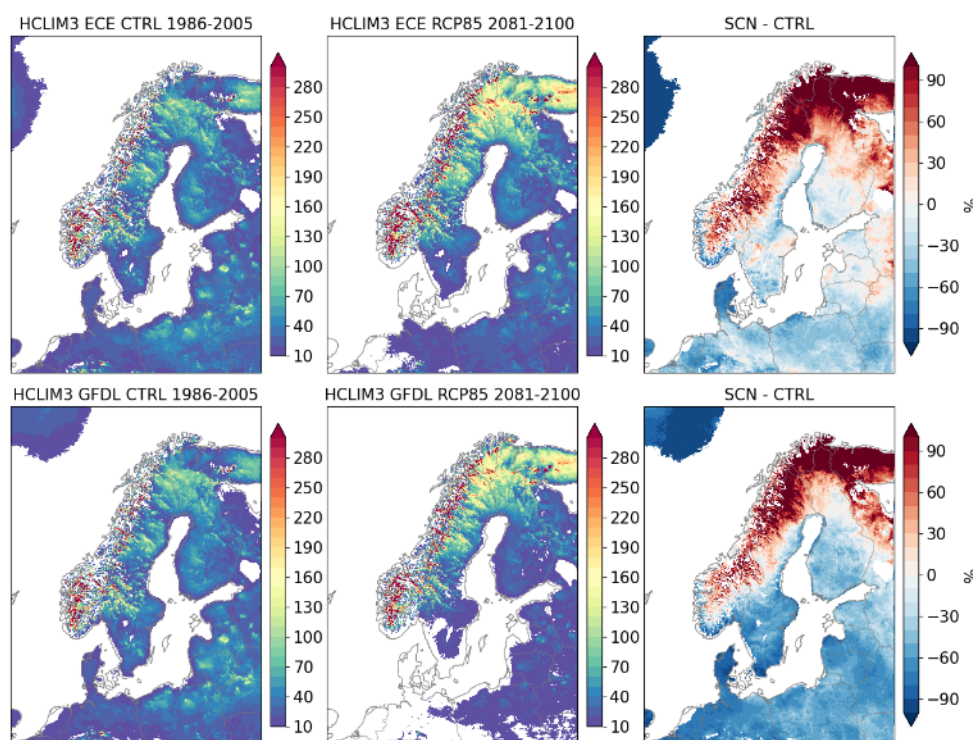
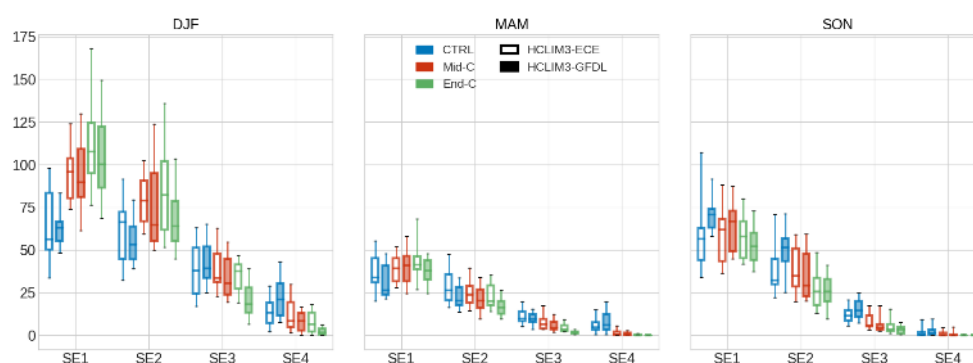


Figure 3.27: As Figure 3.20 but for the number of hours with risk of icing (temperature below 0°C and cloud liquid water content below  $0.5 \cdot 10^{-4}$ ) at the 100-meter level for winter (DJF). Unit: Hours per year (based on 3-hourly instantaneous data).

As summarized for the pricing regions in Figure 3.28 icing is most prominent in the north in winter (DJF) but also appears in spring (MAM) and fall (SON). The gradient from the north to the south is clear with few occasions in the southernmost region and a trend towards even fewer. For the other domains the pattern is more complex. In the northernmost domain both models show increasing trends in winter while for SE2 the models show trends differing in sign, with the EC-Earth-driven simulation indicating larger risk and the GFDL-driven first increasing and then decreasing. For spring decreases are seen in both simulations for SE2, SE3 and SE4. In SE1 there is an increase in the EC-Earth-driven simulation between both periods while, for the GFDL-driven one there is first an increase followed by a decrease at the end of the century. Also, fall shows differences between the two simulations.



**Figure 3.28:** Frequency of days with risk of icing (temperature below  $0^{\circ}\text{C}$  and cloud liquid water content below  $0.5 \cdot 10^{-4}$ ) at the 100-meter level as simulated by HCLIM at 3 km horizontal resolution for the four seasons and the four electricity price areas in Sweden (see Figure 2.1). All numbers are from the RCP8.5 scenario where HCLIM has been taking boundary conditions from EC-Earth and GFDL respectively. The boxes show 25<sup>th</sup> and 75<sup>th</sup> percentiles .... Abbreviations in the legend relates to: CTRL (the historical period 1986-2005), Mid-C (mid-century 2041-2060), End-C (end of century 2081-2100).

### 3.6 CHANGES IN THE LARGE-SCALE CIRCULATION AND IN CIRCULATION TYPES

Here, we make use of the large SLENS ensemble to illustrate potential changes in the large-scale circulation and how it may differ between different ensemble members. Figure 3.29 shows that the ensemble mean large-scale pressure patterns are very similar in the historical and future conditions. However, some differences can be noted as illustrated in Figure 3.30 showing the difference between them, the climate change signal. For winter, higher pressure in much of the area, especially in the north, implies relatively weaker pressure gradients, more high-pressure dominated weather and thereby weaker winds on average. For both spring and fall there are decreases in pressure in the north and increases in the south implying stronger north-south pressure gradients and stronger winds. Areas affected differ between the two seasons with the increase in spring more confined to southern Scandinavia and that in fall found further to the north. For summer, changes are mostly towards lower pressure in all the region implying small changes in pressure gradients and, consequently, only minor changes in wind speed. We note that the climate change patterns for winter (DJF) and summer (JJA) in Figure 3.30 resembles those shown in Figure 1.2 based on a number of EURO-CORDEX simulations.

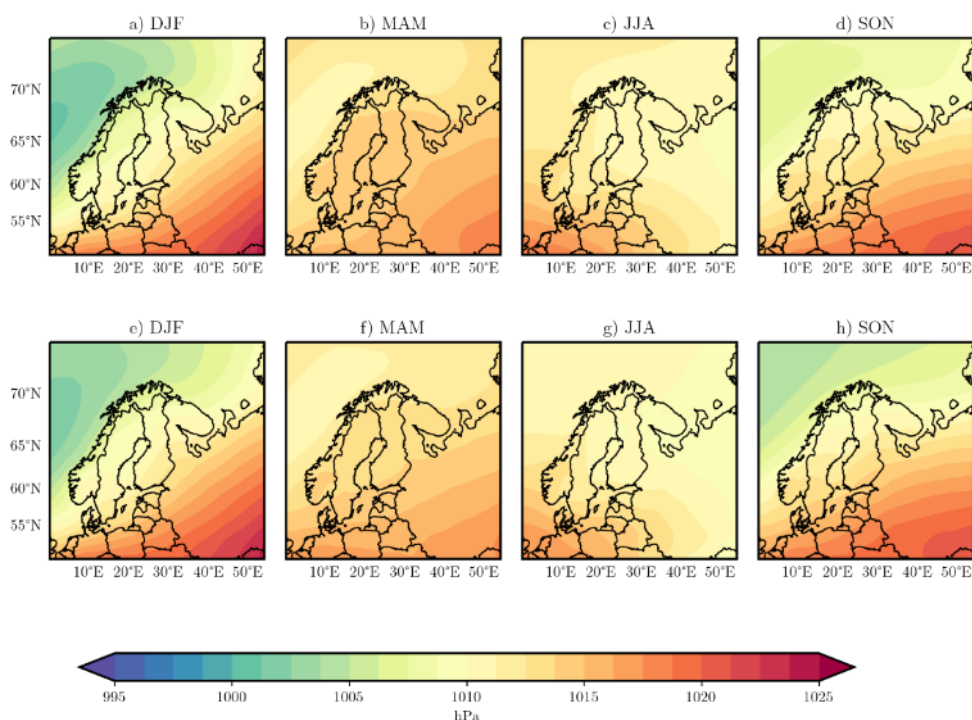


**Figure 3.29: SLENS ensemble mean of mean sea level pressure for the four seasons in the historical climate (top) and for the future SSP5-8.5 scenario in 2071-2100 (bottom).**

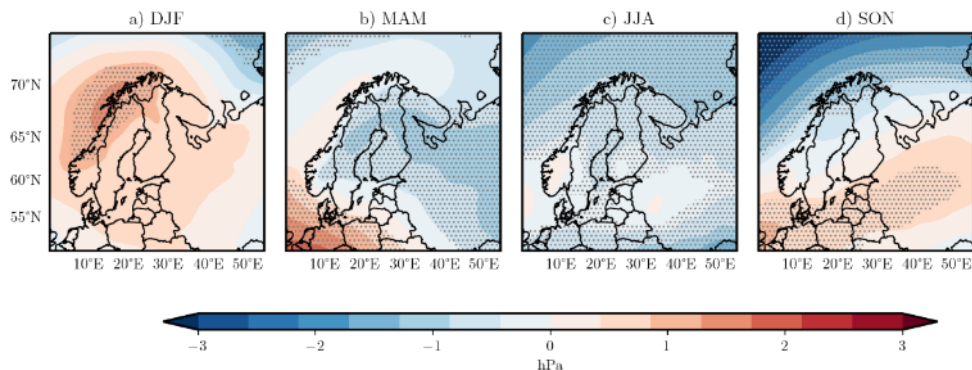


**Figure 3.30: SLENS ensemble mean of the climate change signal in mean sea level pressure from historical to future SSP5-8.5 2071-2100 conditions.**

In Figure 3.31 we look at wintertime changes in mean sea level pressure in all 50 members for winter. The ensemble spans a wide range of potential change patterns. For instance, members r122 and r131 show strong increases in mean sea level pressure in the north, indicating weaker pressure gradients and thereby weaker winds over Scandinavia, while members r124 and r147 show increases in the south indicating stronger pressure gradients and stronger winds. Yet other members, such as r130, show only small or more uniform changes over the area implying only modest changes in the wind climate.

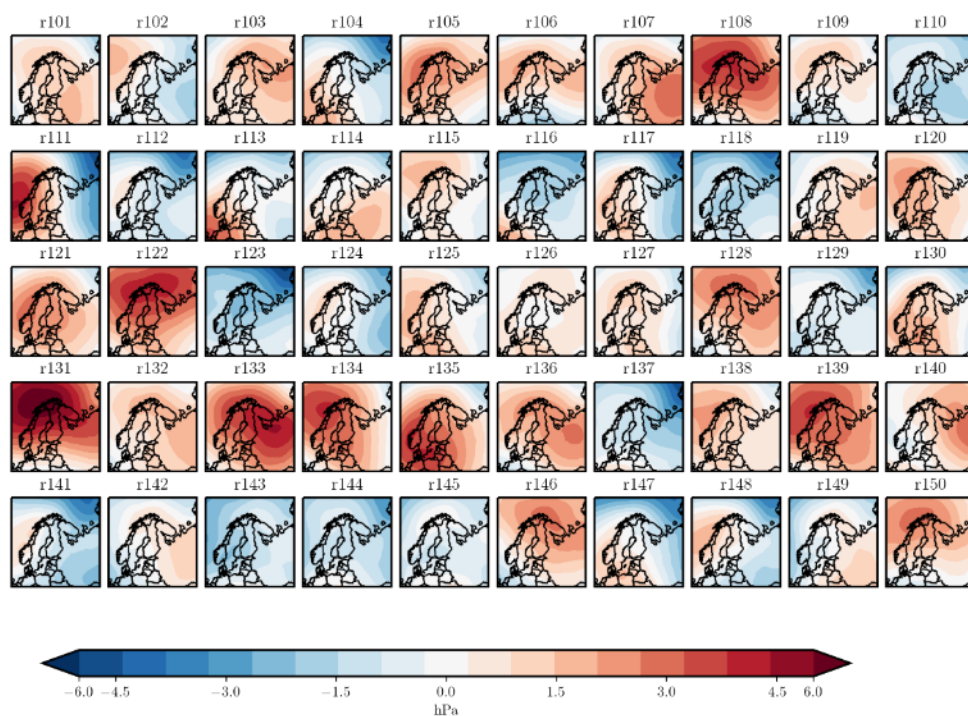


Figure 3.31: As Figure 3.30 but for the individual ensemble members.

Figure 3.32 shows how mean sea level pressure varies over the year in the SLENS ensemble. A bimodal distribution is seen, with highest pressure in May and a secondary maximum in fall. In summer and winter the mean pressure is generally lower. The variability is largest in the winter and smallest in summer. The ensemble mean changes with respect to the historical period are relatively small with exceptions of increases during part of winter and decreases in spring.

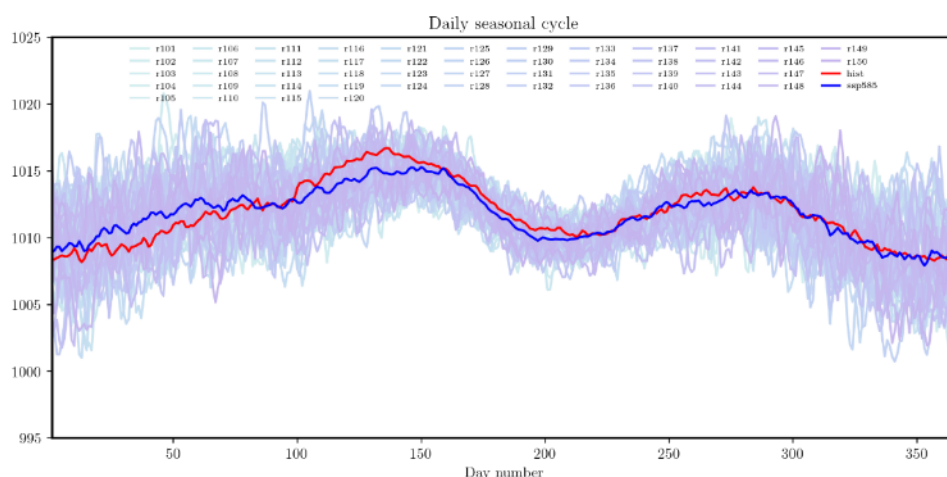


Figure 3.32: Seasonal cycle of mean sea level pressure for the 50-member SLENS ensemble for 2071-2100 under SSP5-8.5. The thick blue line is the ensemble average. Shown is also the ensemble mean from the historical period (thick red line). Unit: hPa.

### 3.7 THE ENERGY SYSTEM AND ITS LINK TO CIRCULATION TYPES

To translate any changes in wind conditions from a warmer climate to impact on energy system level the following steps were taken;

- 1) An electricity system investment model was applied to investigate the cost-optimal electricity system composition for the Nordic countries in a future 2045 using weather data from ten different historical years.
- 2) The prevalence of different circulation types for the ten historical years was assessed.
- 3) The impact of a warmer climate on the prevalence of different circulation types was analysed.
- 4) Combining the understanding of the impact of circulation types on electricity system composition and operation from steps 1-2 with the knowledge of the impact of a warmer climate on prevalence of circulation types the impact of a warmer climate, step 3, on electricity system composition was estimated.

The result of first three steps is presented in the following sections, while the aggregation of the findings in step 4 are presented in the discussion.

#### *Step 1: The impact of historical weather years on the cost-optimal electricity system composition in 2045*

To investigate the impact of circulation types on the optimal electricity system composition and operation the Nordic energy system is modelled for the year 2045 using weather data from ten different historical years as described in Chapter 2.5.

Figure 3.33 shows the simulated cost-optimal installed capacity for electricity production in the region in 2045 given the resources available during the ten years. The same technologies are represented for each year, where solar photovoltaic, gas turbines and on-shore wind turbines (wind class 4 and 5) are allowed to vary with weather conditions while hydropower is set to be constant at today's capacity (see Chapter 2.5). Gas turbines have low investment costs and short start-up time, but high operational costs compared to base load generation, i.e. generation units with high investment cost and low running cost such as nuclear power or coal steam power. This makes gas turbines a cost-efficient complement to wind and solar power.

Figure 3.33 clearly shows that it is cost-efficient to meet the electricity demand in Scandinavia with high wind and solar power together with the existing hydropower. However, there are time periods of low wind speed over most of Scandinavia. Also, there are time periods in which the demand is especially high. For those situations the model suggests that hydropower and gas turbines complement the wind and solar power.

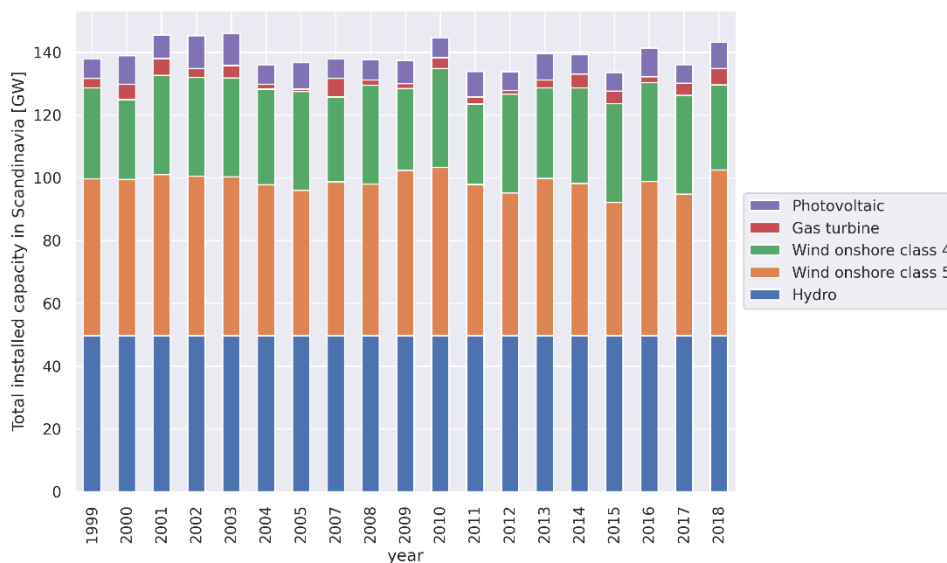


Figure 3.33: Distribution of cost-optimal capacities installed in the region (all ten areas in Figure 2.3) in 2045 as a function of which historical year that has been taken as weather input.

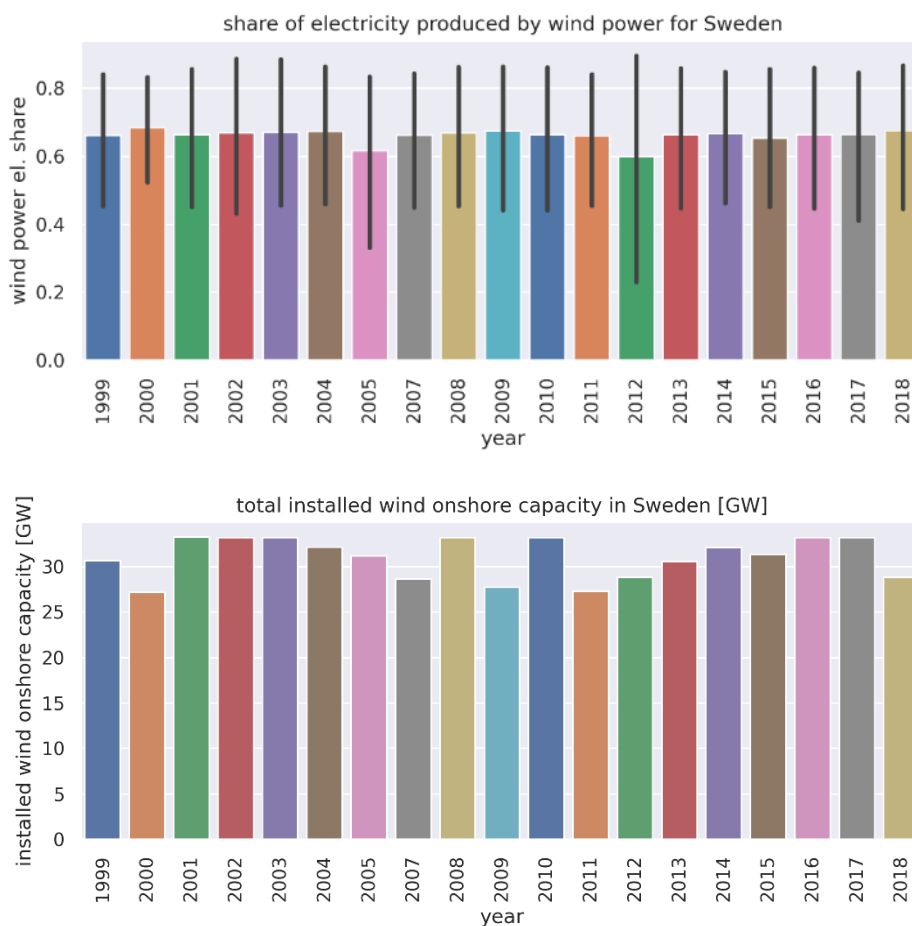


Figure 3.34: electricity share produced by wind power plants (top) and capacity installed in Sweden (bottom). The error bars in the top panel represents the variance between the four regions (SE1 to SE4).

Figure 3.34 (top) shows the electricity share that is produced by wind power in Sweden under the conditions applied in the modeling of this work. The cost-optimal level is around 65% for all years investigated under the assumptions made. Figure 3.34 (bottom), shows the corresponding wind power capacity installed for the same individual years. Relating these two plots, one can conclude that the installed capacity is adjusted between the years to compensate for variations in the wind resource such that wind power meets 65 % of the demand. Thus, the share of electricity demand supplied by wind power is robust across the wind resource variation for the modelled years.

As weather conditions for the years are not identical a more detailed look is given to three of them representing different wind conditions. In Figure 3.35 full load hours (FLH) and hours with low wind power potential (LPP) are visualized for the different regions and the years 2000, 2003 and 2012. In 2003 the FLHs were lower by 8% compared to the other two years. The lower FLH in 2003 results in the need for a higher total installed wind power capacity, as illustrated in Figure 3.34. The amount of FLHs in 2000 and 2012 is relatively similar, with inverse distribution of more FLHs in the south and less in the north for 2012. An inverse relation between the north (SE1 and SE2) and the south (SE3 and SE4) between these two years is seen also for LPP. The good wind conditions in northern Sweden (SE1 and SE2) in 2000 results in high wind power investments in regions SE1 and SE2, with investments also in wind class 4 in SE2. For 2012 there is instead a higher number of low power days in northern Sweden (SE1 and SE2), which result in low incentive to investment in wind power. Hence, very little capacity is installed in SE1 and SE2 year 2012, not even exploiting the whole available wind class 5. A different situation can be seen in southern Sweden (here SE3 and SE4), where FLH are higher in 2012 than in 2000. The relatively small wind resource in northern Sweden (SE1 and SE2) in 2012 results in less class 5 installation possibilities, while heavy investments are suggested in the south (SE3 and SE4). For the southernmost two regions, even exploiting wind class 4 seems to be lucrative. For all 10 regions (Figure 2.3), the average FLH (in parenthesis) of both years, 2000 (4830) and 2012 (4861), is 350-400 hours higher than in the year 2003 (4478).

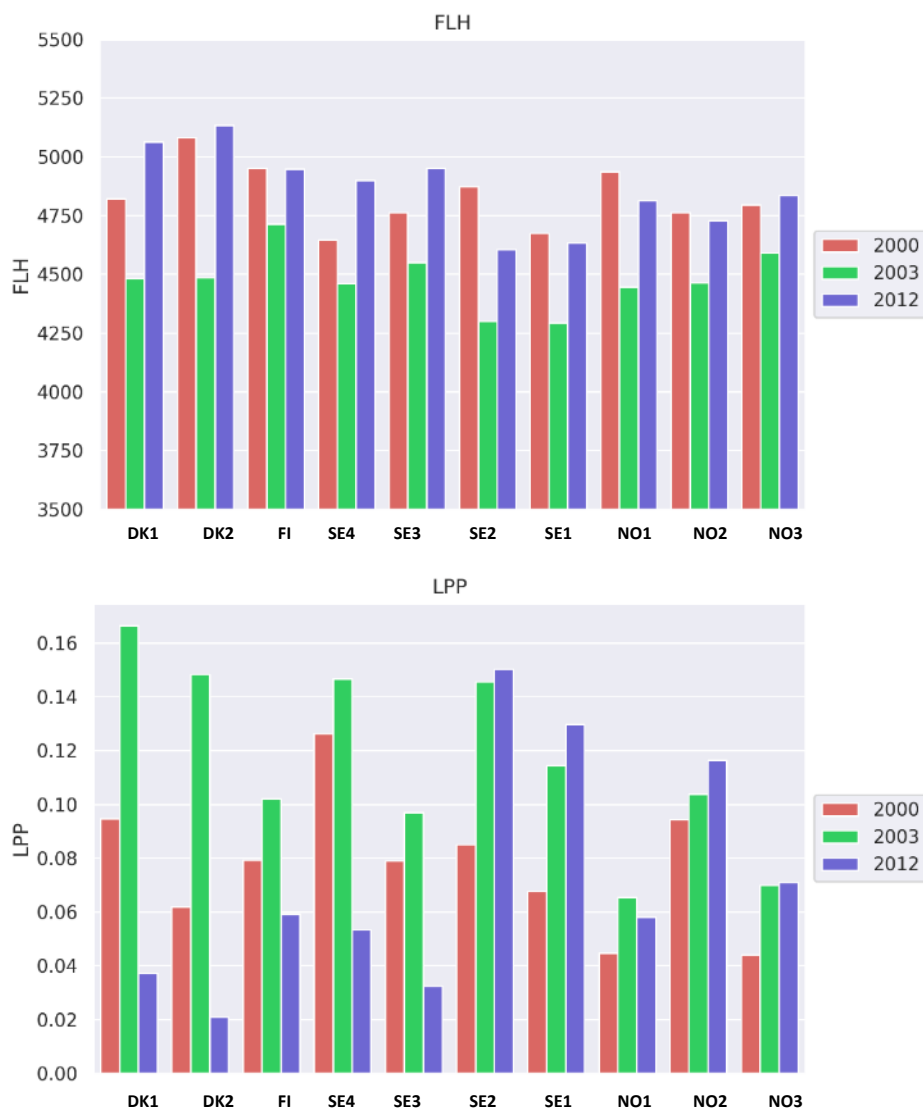
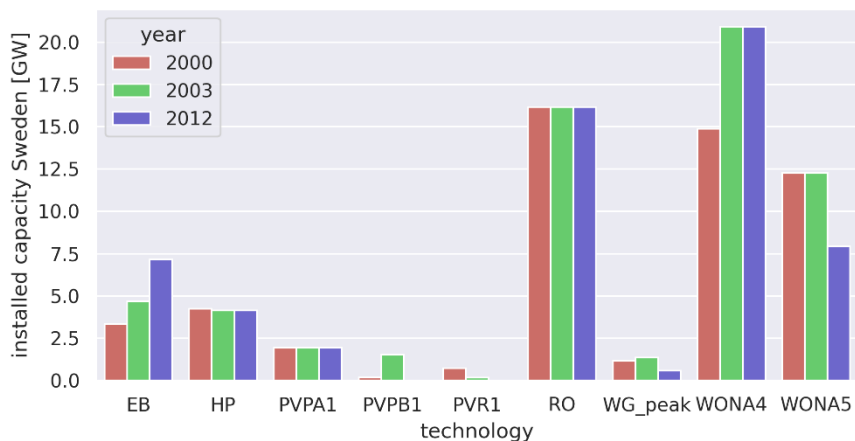


Figure 3.35: Full load hours (FLH) and low power production periods (LPP) per region for 2000, 2003 and 2012.

Figure 3.36 shows that differences in wind conditions also have some impact on how the installed capacity of peaking units with low investment cost such as gas turbines and electric boilers may differ. The smallest installation of total gas turbines is seen for 2012 due to few low wind production periods this year in southern Sweden where the majority of the demand is located. The total electric boiler capacity is highest for the same year since the high FLH in south Sweden in 2012 indicate that wind power is available to a low cost in southern Sweden where the majority of district heating grids are located.



**Figure 3.36: Simulated installed capacity for Sweden (all four pricing areas) in 2045 with wind conditions of 2000, 2003 and 2012. EB (electric boiler), HP (heat pump), PVPA1 (solar photovoltaics located close to grid), PVPB1 (solar photovoltaics located far from grid), PVR1 (rooftop solar photovoltaics), RO (hydropower with storage), WG-peak (biogas open-cycle gas turbine), WONA4 (wind power in wind class 4 -good wind conditions), WONA5 (wind power in wind class 5 -very good wind conditions).**

*Step 2: Connecting historical weather years to circulation types*

As seen above, the differences in wind resources can be linked to atmospheric circulation types. Figure 3.37 gives the distribution of the ten circulation types identified in Chapter 3.2 for all investigated years in the period 1999-2018. It is clear that there is a relatively strong interannual variability with different circulation types being more or less common in the different years. Differences between years can easily be a factor of two to three for most circulation types. The figure also shows that all ten circulation types are present in all years investigated even if some only show up on few occasions in some years (notably circulation type 3 in 2010). The figure is a clear reminder that the climate in Sweden offers highly variable weather conditions with strong differences between the years.

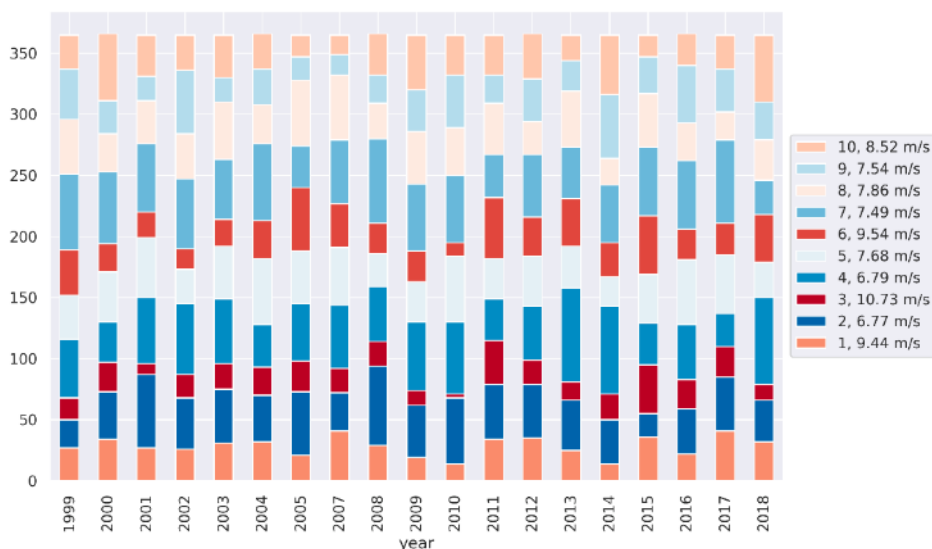


**Figure 3.37: Distribution of number of days per weather regimes during the modelled years. The labels in the legend show the circulation type as depicted in Figure 3.7 and its average wind speed over Scandinavia.**

In Figure 3.38 the four dominant winter and summer circulation types (cf. Figure 3.8) are displayed for the years 2000, 2003 and 2012. In 2003, that is the year with the least wind resource and thereby largest need for installed capacity (cf. Figure 3.34) it can be noted that the windier circulation types 1, 3, 6 and 10 are less frequent compared to the other two years.

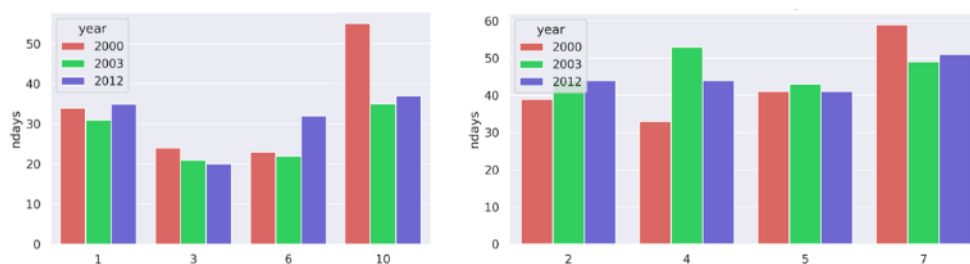


**Figure 3.38:** Number of days a wind regime WR occurs during the year. The left panel shows the typical “winter” circulation types. The right one shows the “summer” types.

### *Step 3: The impact of a warmer climate on the circulation types*

The S-LENS results presented in Chapter 3.6 indicate that there are relatively modest systematic changes related to the large-scale circulation in the future (Figure 3.30 and 3.32) although individual ensemble members show strong differences (Figure 3.31). In another study on S-LENS results analyzing changes in a similar, albeit not identical, set of ten different circulation types as the ones discussed in Chapter 3.2, Hansen et al. (2023) show that there are no strong future changes to be expected in the pressure patterns connected to the identified circulation types. They also found only relatively small changes for the frequencies of the circulation types. The most significant changes were identified for the summer half-year. In particular, they found a decrease in May in the circulation type with a high-pressure ridge from Finland towards the southwest (corresponding to circulation type 9 in Figure 3.7).

In any single climate simulation for the future, and in reality, natural variability is relevant and we expect to see deviations from the long-term (small) trends. Figure 3.39 shows the change in frequencies of the circulation types (defined in Chapter 3.2) between the HCLIM historical and mid-century simulations assessed in Chapter 3.4. The two figures indicate that the large-scale patterns remain very similar with certain circulation types dominating in different seasons. Differences between the two periods are from a few percent up to 20-30% for some circulation types. We note that this is substantially lower than the interannual variability shown in Figure 3.37.

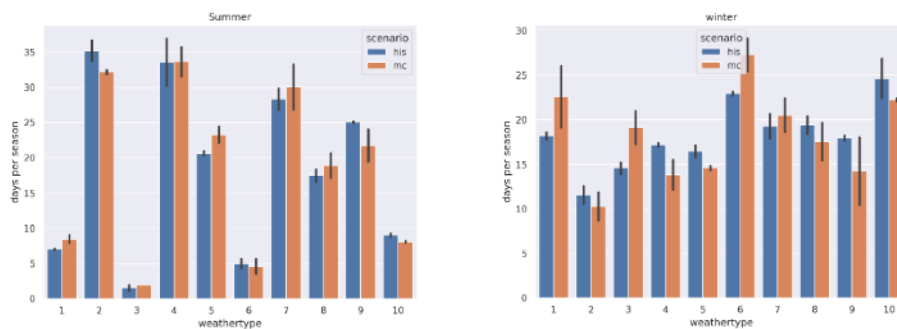


Figure 3.39: Frequency of circulation types for the historical period (1998-2018) and the mid-century period (2040-2060) in the HCLIM simulation with EC-Earth under RCP8.5. The panels show conditions for the extended summer (left) and winter (right) seasons.

## 4 Discussion

### 4.1 REPRESENTATIVITY OF MODELS

We have seen (Chapter 3.4) that the two simulations with HCLIM driven by two different GCMs differ significantly in how they represent future changes in the wind climate. As the results are based only on these two simulations they are likely not representative of the full uncertainty related to future climate change (cf. Chapter 1.2). In order to set the results in a wider perspective we illustrate how the wind climate may change by looking at three different large ensembles of climate models: i) the CMIP6 global climate models under the SSP5-8.5 scenario, ii) the EURO-CORDEX regional climate models under the RCP8.5 scenario and iii) the SLENS ensemble consisting of 50 members with the EC-Earth model under the SSP5-8.5 scenario.

Table 4.1 shows relative wind speed changes in the CMIP6 and EURO-CORDEX ensembles, both in terms of median and in terms of spread between the individual ensemble members (5<sup>th</sup> and 95<sup>th</sup> percentiles). Data are taken from the IPCC Interactive Atlas and are representative for land areas in Northern Europe (approximately the British Isles, Scandinavia and Finland). Here, we have chosen to present the scenario with the strongest forcing (SSP5-8.5 / RCP8.5) to be comparable with the HCLIM results. The table presents climate change signals for three different levels of global warming: +1.5°C representing the near future, +2°C representing decades around or after mid-century and +4°C representing the end of the century or beyond. In scenarios with weaker forcing (such as SSP2-4.5 / RCP4.5 and SSP1-2.6 / RCP2.6) these warming levels are reached later if at all.

**Table 4.1** Future change in surface wind speed averaged over land areas in northern Europe. Numbers are shown for time periods when the global mean temperature has increased with 1.5, 2.0 and 4.0°C relative to preindustrial conditions (1850-1900). Changes are given relative to 1995–2014. The numbers represent median change among the models and, in parenthesis, the 5th and 95th percentiles. Data is taken from the IPCC interactive atlas<sup>8</sup> (Iturbide et al., 2021 and Gutiérrez et al., 2021).

Ensemble of simulations (number of ensemble members)	Change in wind speed (%) (+1.5°C)	Change in wind speed (%) (+2°C)	Change in wind speed (%) (+4°C)
<i>Winter (DJF)</i>			
EURO-CORDEX RCP8.5 (48)	-0.8 (-2.9 – 1.2)	-0.0 (-3.7 – 3.2)	0.2 (-3.6 – 3.1)
CMIP6 SSP5-8.5 (31)	0.2 (-3.3 – 4.1)	0.1 (-4.3 – 5.0)	-0.2 (-6.9 – 4.1)
<i>Spring (MAM)</i>			
EURO-CORDEX RCP8.5 (48)	0.4 (-2.1 – 3.5)	-0.4 (-2.1 – 1.6)	-1.1 (-2.7 – 1.6)
CMIP6 SSP5-8.5 (31)	-0.2 (-3.0 – 2.9)	-0.6 (-4.5 – 3.3)	-1.1 (-4.7 – 2.9)
<i>Summer (JJA)</i>			
EURO-CORDEX RCP8.5 (48)	-0.7 (-2.0 – 0.6)	-0.7 (-2.4 – 1.4)	-1.8 (-4.4 – 0.0)
CMIP6 SSP5-8.5 (31)	-0.8 (-2.9 – 1.6)	-1.3 (-5.1 – 1.6)	-4.2 (-9.5 – 0.4)
<i>Fall (SON)</i>			
EURO-CORDEX RCP8.5 (46)	0.1 (-1.4 – 1.4)	0.0 (-2.0 – 1.5)	0.4 (-1.8 – 2.7)
CMIP6 SSP5-8.5 (31)	-0.7 (-5.0 – 1.8)	-0.6 (-3.8 – 2.2)	-1.4 (-5.0 – 1.8)

<sup>8</sup> See <https://interactive-atlas.ipcc.ch/>

The numbers in the table clearly show that there is a large-scale tendency towards lower wind speed in the summer half of the year. Notably, the CMIP6 models show ensemble median decreases for all time periods and seasons except winter. For the CORDEX ensemble the negative trend is more confined to summer and in the later periods also spring. Most median changes are within  $\pm 1\%$  apart from at  $4^\circ\text{C}$  global warming when decreases in summer are larger. We also note that, for all seasons and time periods the 5<sup>th</sup> to 95<sup>th</sup> percent interval encompasses zero indicating that there are simulations showing either decreasing or increasing wind speed with generally up to  $\pm 5\%$  on a seasonal mean basis. This corresponds to about 15% differences in wind power potential, which can be compared with the numbers derived for the two experiments with HCLIM discussed above.

What can be learned from large ensembles such as those in Table 4.1 or the 50-member S-LENS ensemble discussed above? Is the ensemble mean changes what we can expect to see in the future? In reality, there is of course only one “ensemble member” – the actual climate evolution. If the ensemble mean change (signal) is strong compared to the individual response in the ensemble members (noise), the models indicate that there is a strong chance that such a change may occur in the future. If, however, the signal-to-noise ratio is low, any long-term trends would likely be masked by the (natural) variability. This means that for any particular time period of 20 to 30 years, results may differ strongly from what the ensemble mean indicates. To understand what future changes may look like it is therefore a good idea to analyze not just ensemble means from large ensembles but also the spread between individual ensemble members.

## 4.2 IMPACTS OF CLIMATE CHANGE ON THE ENERGY SYSTEM

Even though the available wind resource varies between the 20 years investigated, the results presented here (Chapter 3.7) show that this has low impact on the role of wind power in the electricity system. For all years investigated, wind power cost-efficiently supplies around 65 % of the demand for electricity, both in Sweden and in the Nordic countries as a whole. The total installed capacity of wind power is adjusted to compensate for variations in wind conditions such that this amount of the electricity demand can be met by wind power.

As a consequence, the changing wind conditions between years has a low impact on the cost-optimal installed capacity of other types of electricity generation units. Only the installed capacity of peaking units, with low investment cost, vary between the years investigated.

A clear correlation between circulation types and wind power full load hours and low production periods could be identified. However, if climate change is to have an impact on the role of wind power in the electricity system, the change of average number of days of the circulation types between today and in a warmer climate must be greater than the difference between any two years between 1999-2018. This is not expected as illustrated by the analysis of circulation types in S-LENS discussed in Chapter 3.6.

The consequences of variations in wind conditions between the historical years were to some extent reduced by the possibility to change location of wind power investments between the years investigated. Based on the variations in wind conditions at different geographical location a distribution of installed wind power capacity between regions adapted to the occurrence of different circulation types together with good conditions for electricity trade is recommended.

## 5 Conclusions

The results presented here supports the picture of strongly varying wind conditions in Sweden and Northern Europe. Historic variation between years and regions are quite large. Despite this variability, we find that the total integrated wind resource over large areas, such as Northern Europe, is relatively robust. Considering the equalizing effect of spreading wind turbines over a large geographical area implies that fluctuations in wind energy production between years can be substantially decreased. An example shows that the annual production for individual wind power areas varied approximately  $\pm 15\%$  between individual years over the last decade. In this case, the variation was reduced to approximately  $\pm 7\%$  when including 51 locations over northern Europe. For shorter time scales, however, there are periods, in all seasons, with low wind conditions also as integrated over large areas.

Categorizing the wind conditions dependent on large-scale circulation types is found to be a good way to illustrate the wind variability in the region. Different wind conditions in different circulation types include: not just, lower than average wind speed in high pressure situations and higher than average wind speed in low-pressure dominated ones; but also, geographical differences between different regions. There are clear differences in the circulation types between summer and winter. Differences in frequencies of the analysed circulation types can be used to categorize different years in both total wind power potential and conditions for low wind production.

Large climate model ensembles indicate a large amount of variability in the wind climate, from year to year and from decade to decade. This large natural variability makes it difficult to depict any coherent change in the future wind climate. Judging from the relatively small future changes in different circulation types in a large ensemble of simulations, only small changes are expected in the wind climate. The most prominent change as derived from large ensembles of climate models is that wind speed in summer may decrease in the future in parts of northern Europe. For other seasons, and also for summer, the variation between models is large. This implies that even on timescales of 20-30 years there are scenarios showing either increases or decreases in the wind power potential in Northern Europe with large geographical differences.

We evaluate a high-resolution regional climate model operated at 3 km grid spacing over Scandinavia. When the model is forced by reanalysis data it provides clear added value compared to other, coarse resolution models commonly used for climate impact studies. In particular, altitude-related features of the wind climate are better resolved in the fine-scale model. Comparison to observations, both at the 10-meter level and at hub height, show generally good agreement. This relates both to geographical variations and temporal variations, such as the annual and daily cycles. An underestimation of high wind speed compared to point measurements (weather stations and wind turbines) is found. The general good agreement to observations lends confidence to the use of such a high-resolution climate model to provide information about variations and change in the wind climate over Scandinavia.

The high-resolution scenarios for future wind conditions derived by the 3-km regional climate model depicts two very different future states with one of the scenarios indicating strong wind speed increases while the other one shows only small changes. Geographical details of the changes are found to depend strongly on changes in large-scale forcing by the underlying global models. There are, however, regional details in the change signals that may be related to local changes in temperature and/or vertical stability. Here, reduced snow on the ground leading to higher near-surface temperatures would reduce the potential to form strong high-reaching inversions in valleys and thereby causing systematic decreases in the number of days with low wind speed in some areas.

A warmer climate generally leads to less days with snow and ice as the summer season gets longer. However, results from the high-resolution 3-km model indicate that icing-related problems may increase in a warmer climate in Scandinavia during parts of the year. A gradually warmer winter climate will, in cold areas, involve more days with temperatures closer to zero degrees and higher moisture content compared to the colder conditions with low moisture content in today's climate. Many areas may therefore first see more icing-related problems during the cold season before the situation eventually gets less prone to icing. In some regions, such as the mountains and interior parts of northern Sweden, a future warmer climate is more favourable of icing also at the end of the century even under scenarios of strong warming.

Energy system model results indicate that a future energy system with a larger fraction of wind power is relatively robust to internal variability in weather conditions for year-to-year variations. Also, the results show that there is a low impact on the cost-optimal installed capacity of other types of electricity generation units. Taken together the results show that it is cost-efficient to meet the electricity demand in Scandinavia with high wind and solar power together with the existing hydropower. For situations with low wind speed over most of Scandinavia the model suggests that hydropower and gas turbines complement the wind and solar power.

## 6 References

- Belušić D, de Vries H, Dobler A et al. 2020. HCLIM38: A flexible regional climate model applicable for different climate zones from coarse to convection-permitting scales. *Geosci. Model Dev.*, 13, 1311–1333, doi:10.5194/gmd-13-1311-2020.
- Blomqvist P, Gode J, Kjellström E et al. 2021. Klimatförändringarnas inverkan på vindkraften. *Energiforsk rapport nr 2021:742*, ISBN 978-91-7673-742-2, 45 pp.
- Blomqvist P, Unger T, Odenberger M et al. 2023. Vindkraftens sammanlagring i Norra Europa - Validering av modelldata, samt analys av hur vindkraftsproduktion varierar över norra Europa. *Energiforsk rapport nr 2023:938*, ISBN 978-91-7673-938-9, 53 pp.
- Bärring L and von Storch H, 2004. Scandinavian storminess since about 1800, *Geophys. Res. Lett.*, 31, L20202, doi:10.1029/2004GL020441.
- Christensen OB, Kjellström E, Dieterich C et al. 2022. Atmospheric regional climate projections for the Baltic Sea Region until 2100. *Earth Syst. Dynam.*, 13, 133-157, DOI:10.5194/esd-13-133-2022.
- Claussen N, Lundsager P, Barthelmie R et al. 2007. Wind power. In: Fenger, J (ed.). *Impacts of climate change on renewable energy sources: Their role in the Nordic Energy System*. Nord 2007:003. ISBN 978-92-893-1465-7.
- Claussen N, Larsén XG, Pryor SC et al. 2011. Wind power. In: Thorsteinsson, T. and Björnsson, H. (eds). *Climate change and energy systems: Impacts, risks and adaptation in the Nordic and Baltic countries*. TemaNord 2011:502. Nordic Council of Ministers, Copenhagen. 226 pp. ISBN 978-92-893-2190-7.
- Dee DP, Uppala SM, Simmons AJ et al., 2011. The ERA-Interim reanalysis: configuration and performance of the data assimilation system. *Q J R Meteorol Soc* 137:553–597, doi:10.1002/qj.828
- Deser C, Lehner F, Rodgers KB et al., 2020. Insights from Earth system model initial-condition large ensembles and future prospects. *Nat. Clim. Chang.* 10, 277–286, doi:10.1038/s41558-020-0731-2
- DNA, 2016. ENS, Technology Data - Energy Plants for Electricity and District heating generation. Danish Energy Agency and Energinet.
- Energimyndigheten, 2023. Myndighetsgemensam uppföljning av samhällets elektrifiering. *Rapportering 2022, ER 2023:02*, Energimyndigheten, 631 04 Eskilstuna, ISBN 978-91-7993-105-6, 48 pp.
- Eyring V, Bony S, Meehl GA et al. 2016 Overview of the Coupled Model Intercomparison Project Phase 6 (CMIP6) experimental design and organization *Geosci. Model Dev.* 9 1937–58.
- Gelaro R, McCarty W, Suárez MJ et al., 2017. The Modern-Era Retrospective analysis for research and applications, version 2 (MERRA-2). *Journal of Climate*, 30(13), 5419–5454, doi:10.1175/JCLI-D-16-0758.1

Gutiérrez JM, Jones RG, Narisma GT et al. 2021 Atlas. In *Climate Change 2021: The Physical Science Basis. Contribution of Working Group I to the Sixth Assessment Report of the Intergovernmental Panel on Climate Change* [Eds. Masson-Delmotte V, Zhai P, Pirani A, et al]. Cambridge University Press. In Press. Interactive Atlas available from Available from <http://interactive-atlas.ipcc.ch/>

Göransson L, Goop J, Odenberger M et al. 2017. Impact of thermal plant cycling on the cost-optimal composition of a regional electricity generation system. *Applied Energy*, 197, 230-240, doi:10.1016/j.apenergy.2017.04.018

Hansen F and Belušić D 2021. Tailoring circulation type classification outcomes. *Int. J. Climatol.*, 41(14): 6145–6161. DOI: <https://doi.org/10.1002/joc.7171>

Hansen F, Belušić D, Wyser K et al. 2023. Future changes in circulation types and their effects on surface air temperature and precipitation in the SMHI large ensemble. *Clim. Dyn.*, doi:10.1007/s00382-023-06704-y

Hersbach H, Bell B, Berrisford P, et al., 2020. The ERA5 global reanalysis. *Q J R Meteorol Soc.* 146, 1999– 2049, doi:10.1002/qj.3803

Holttinen H. 2003. Hourly Wind Power Variation and Their Impact on the Nordic Power Operation. Ph.D. Thesis, Helsinki University of Technology, Espoo, Finland.

Hovsenius G and Kjellström E, 2007. Konsekvenser för vindkraften i Sverige av klimatförändringar. *Elforsk rapport nr 07:33*, 42 pp.

IEA, 2022. *Global Energy and Climate Model Documentation 2022*, International Energy Agency (IEA), Paris, <https://www.iea.org/reports/global-energy-and-climate-model>, License: CC BY 4.0, 124 pp.

IPCC, 2021. Summary for Policymakers. In: *Climate Change 2021: The Physical Science Basis. Contribution of Working Group I to the Sixth Assessment Report of the Intergovernmental Panel on Climate Change* [Masson-Delmotte V et al. (eds.)]. Cambridge University Press, Cambridge, United Kingdom and New York, NY, USA, pp. 3–32, doi:10.1017/9781009157896.001.

IPCC, 2022a. Summary for Policymakers. In: *Climate Change 2022: Impacts, Adaptation, and Vulnerability. Contribution of Working Group II to the Sixth Assessment Report of the Intergovernmental Panel on Climate Change* [Pörtner H-O, et al. (eds.)]. Cambridge University Press, Cambridge, UK and New York, NY, USA, pp. 3-33, doi:10.1017/9781009325844.001.

IPCC, 2022b. Summary for Policymakers. In: *Climate Change 2022: Mitigation of Climate Change. Contribution of Working Group III to the Sixth Assessment Report of the Intergovernmental Panel on Climate Change* [Shukla, PR, et al. (eds.)]. Cambridge University Press, Cambridge, UK and New York, NY, USA, doi: 10.1017/9781009157926.001

Iturbide M, Fernández J, Gutiérrez JM et al. 2021. Repository supporting the implementation of FAIR principles in the IPCC-WG1 Atlas. Zenodo, DOI: 10.5281/zenodo.3691645. Available from: <https://github.com/IPCC-WG1/Atlas>

- Jacob D, Teichmann C, Sobolowski S et al. 2020. Regional climate downscaling over Europe: perspectives from the EURO-CORDEX community. *Reg. Environ. Change*, 20:51, doi:10.1007/s10113-020-01606-9.
- Johansson V and Göransson L, 2020. Impacts of variation management on cost-optimal investments in wind power and solar photovoltaics. *Renewable Energy Focus*, 32, 10-22, doi:10.1016/j.ref.2019.10.003
- Johansson V, Thorson L, Goop J et al. 2017. Value of wind power – Implications from specific power. *Energy* 126, 352-360, doi:10.1016/j.energy.2017.03.038
- Kjellström E, Nikulin G, Strandberg G et al. 2018. European climate change at global mean temperature increases of 1.5 and 2 °C above pre-industrial conditions as simulated by the EURO-CORDEX regional climate models, *Earth Syst. Dynam.*, 9, 459-478, DOI: 10.5194/esd-9-459-2018.
- Kjellström E, Hansen F and Belušić D 2022. Contributions from changing large-scale atmospheric conditions to changes in Scandinavian temperature and precipitation between two climate normals. *Tellus A: Dynamic Meteorology and Oceanography*, 74, 204–221. DOI:10.16993/tellusa.49
- Kringlebotn Nygaard BE, Kristjánsson JE and Makkonen L. 2011. Prediction of in-cloud icing conditions at ground level using the WRF model. *J. Appl. Met. Clim.* 50(12), 2445-2459. doi:10.1175/JAMC-D-11-054.1.
- Lind P, Belušić D, Christensen OB et al. 2020. Benefits and added value of convection-permitting climate modeling over Fenno-Scandinavia. *Clim. Dyn.* 55, 1893–1912. Doi:10.1007/s00382-020-05359-3.
- Lind P, Belušić D, Médus E et al. 2022. Climate change information over Fenno-Scandinavia produced with a convection-permitting climate model. *Clim. Dyn.* doi:10.1007/s00382-022-06589-3
- Mattsson N, Verendel V, Hedenus F et al. 2021. An autopilot for energy models – automatic generation of renewable supply curves, hourly capacity factors and hourly synthetic electricity demand for arbitrary world regions. *Energy Strategy Reviews*, 33, 100606, doi:10.1016/j.esr.2020.100606.
- Meier HEM, Kniebusch M, Dieterich C et al. 2022. Climate change in the Baltic Sea region: a summary, *Earth Syst. Dynam.*, 13, 457–593, doi:10.5194/esd-13-457-2022.
- Olauson J. Modelling Wind Power for Grid Integration Studies. Doktorsavhandling, Uppsala universitet 2016, ISSN 1651–6214.
- Reichenberg L, 2017. Variability and variation management in a renewable electricity system - large-scale wind- and solar power deployment in Europe. Doktorsavhandling, Chalmers, ISBN 978-91-7597-646-4.
- Reichenberg L, Johnsson F and Odenberger M, 2014. Dampening variations in wind power generation - The effect of optimizing geographic location of generating sites. *Wind Energy*, 17(11): 1631-1643.

Rutgersson A et al. 2015. Recent Change—Atmosphere. In: The BACC II Author Team (eds). Second Assessment of Climate Change for the Baltic Sea Basin. Regional Climate Studies. Springer, Cham., doi:10.1007/978-3-319-16006-1\_4

Rydblom S and Thörnberg B, 2020. Measurement of Atmospheric Icing and Droplets. IEEE Transactions on Instrumentation and Measurement, 69(8), 5799-5809, doi: 10.1109/TIM.2020.2966313.

Scharff R, Göransson L, Walter V et al. 2023. Klimatförändringarnas inverkan på vattenkraftens produktions- och reglerförmåga. Energiforsk: 2023:924 Stockholm. ISBN 978-91-7673-924-2, pp 117.

Schimanke S, Joelsson M, Andersson S et al. 2022. Observerad klimatförändring i Sverige 1860–2021. Klimatologi 69, SMHI, SE-60176 Norrköping. ISSN: 1654-2258, 77 pp.

Van der Wiel K, Bloomfield HC, Lee RW et al. 2019. The influence of weather regimes on European renewable energy production and demand. Environ. Res. Lett. 14, 094010, doi:10.1088/1748-9326/ab38d3

Wiser R and Bolinger M, 2015. 2014 wind technologies market report. Oak Ridge: U.S. Department of Energy.

Wyser K, Koenigk T, Fladrich U et al. 2021. The SMHI Large Ensemble (SMHI-LENS) with EC-Earth3.3.1, Geosci. Model Dev., 14, 4781–4796, doi:10.5194/gmd-14-4781-2021.

WMO, 2023. State of the Global Climate 2022 (WMO-No. 1316). Geneva, Switzerland. ISBN 978-92-63-11316-0, pp 49.

## 7 Appendix

### 7.1 GIS PARAMETERS FOR ONSHORE / OFFSHORE WIND POWER

To translate wind speeds to wind power the GIS-based analysis tool developed by Mattsson et al. (2021) is applied. In the following the assumptions and parameters chosen for the GIS analysis are listed. The presentation of data is aligned with the supplementary data of the corresponding model description in the supplementary material in [7]. Note, that only the parameters deviating from the default parameters are listed.

*Area & capacity assumptions:*

1. onshore share of remaining area available for wind farms: 100%
2. offshore share of remaining area available for wind farms: 100%

Note that in this study the limitation of the available area is not set in the GEGIS package, hence the parameter is set to 100%. For post-analysis of the wind power and implementation in the energy system model these parameters are set to 10% and 33%, respectively for on- and offshore wind.

*Mask assumptions:*

1. maximum water depth for offshore wind: 50 m
2. minimum distance to shore for offshore wind: 2 km

Note, that in this study it is assumed that all installations are close to a grid, so the the capacity of class A and class B wind turbines are added to one single value. The time-series are taken from class A.

*Resource class assumptions:*

In this study only one offshore class is used (Table 7.1), considering only a wind class describing high wind speeds. This limitation has no impact on the results as the optimal solution of an energy system run would not include any investments in lower offshore wind class than five.

**Table 7.1: Wind speed intervals for wind classes.**

Wind class	Onshore (m/s)	Offshore (m/s)
class 1	2-5	-
class 2	5-6	-
class 3	6-7	-
class 4	7-8	-
class 5	8+	8+

### Wind turbine and park output curves

In order to convert instantaneous wind speeds to the capacity factors a power output profile of a Siemens Gamesa G114 2.1 MW wind turbine. The turbine is chosen due to its specific power of 200 W/m<sup>2</sup>. The specific power of a wind turbine is defined as

$$P_{\text{spec}} = \frac{\text{rated power}}{\text{rotor area}} = \frac{W}{m^2}.$$

The power curve of a single turbine is formulated as

$$P_{\text{WT,ind}}(v_w) = \begin{cases} \eta_{\text{ext}} \min \left( \eta_{\text{int}} \frac{1}{2} c_p(v_w) \frac{\pi}{4} D^2 \rho v_w^3, P_{\text{cap}} \right) \frac{1}{P_{\text{cap}}} & \text{for } v_{\text{in}} \leq v_w \leq v_{\text{out}} \\ 0 & \text{otherwise} \end{cases},$$

where the rotor diameter is  $D = 100$  m and the generator size is  $P_{\text{cap}} = 1.94$  MW, assuming the specific power of the wind turbine is 247 W/m<sup>2</sup>. The internal and external losses are  $\eta_{\text{int}} = 0.885$  and  $\eta_{\text{ext}} = 0.94$ , respectively. The efficiency  $c_p$  is a function of the wind speed  $u_w$ . The cut-in and cut-out wind speeds  $v_{\text{in}}$  and  $v_{\text{out}}$  are assumed to be 3 and 25 m/s, respectively.

Compared to Eq. (1) the power of a wind farm is assumed to be smoothed due to the normally distributed wind speeds in a farm. Here a standard deviation of  $\sigma = 1$  m/s is used. The normalized instantaneous power produced by a farm is thus computed as

$$P_{\text{WT,farm}}(v_w) = \int_0^{30} f(x|v_w, \sigma^2) P_{\text{WT,ind}}(x) dx,$$

where  $f$  is the probability density function of the normal distribution. The standard deviation smooths the power generation curve at the cut-in and cut-out wind speeds. The effect for the wind turbine power curve is visualized in Figure 7.1.

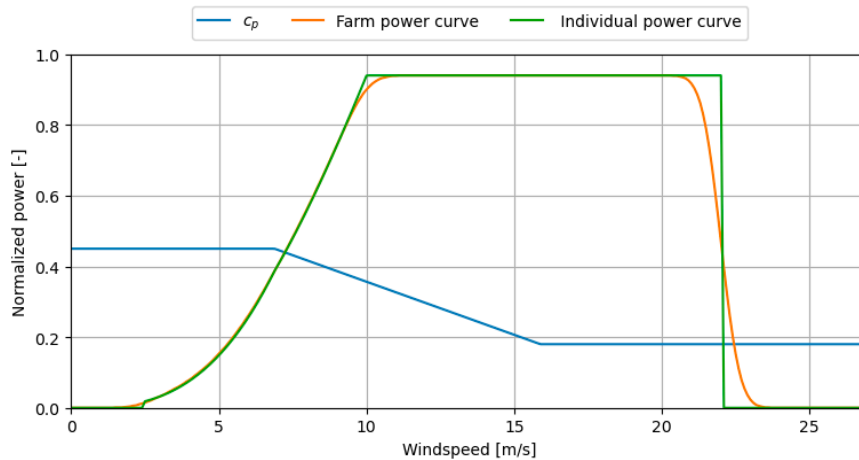


Figure 7.1: Power curve of an individual wind turbine and of a wind farm with a standard distribution of the wind speed of  $\sigma = 1$  m/s. The greater the standard distribution, the greater the smoothing effect. The power curve is limited to 94% to account for wind farm losses and maintenance downtime.

The farm power density  $\rho_{P,WT}$  of the WT farm is defined by the spacing of the wind turbines. In this study, the distance between the turbines is chosen to be seven times the rotor diameter, such that an area of  $7D \times 7D$  is used for one turbine. This distance dependency is due wake and shadowing effects of neighbouring turbines. Given the specific power of the wind turbines of  $247 \text{ W/m}^2$ , this results in a farm power density of  $3.95 \text{ MW/km}^2$ .

## 7.2 TECHNOLOGY DATA FOR THE ENERGY SYSTEM MODEL

Table 7.2: Costs and technical data for the electricity generation technologies.

Technology	Investment cost [M€/MW(h)]	Variable O&M costs [€/MWh]	Fixed O&M costs [k€/MW, yr]	Life-time [yr]	Efficiency [%]
Biomass ST	2.0	2.1	52	40	35
Biogas CCGT	0.90	0.8	17	30	61
Biogas GT	0.45	0.4	15	30	42
Nuclear	4.0	6.6	95	60	33
Solar PV	0.3	0.5	7	40	100
Onshore wind	1.0	1.1	13	30	100
Offshore wind	1.5	1.1	36	30	100
Heat pump	0.9	2.2	2	25	3
Electric boiler	0.1	1	1	20	1

Table 7.3: Costs and technical data for storage technologies. The power to energy ratio of the storages are assumed to equal 1, i.e. the storages can be discharged in 1h.

Storage technology	Investment cost [M€/ MWh]	Efficiency (charge/discharge) [%]	Fixed O&M costs [k€/MW(h), yr]	Life-time [yr]
Battery, Li-ion	0.15	96/96	0.5	25
Tank heat storage	0.003	100/1	0.009	25

1) Heat storages have a continuous loss corresponding to 0,023 % per unit of time and energy stored

Table 7.4: Costs and for the fuels used in this study.

Fuel types	Fuel cost [€/MWhth]
Biomass	40
Biogas	77
Uranium	3.0

# IMPACT OF CLIMATE CHANGE ON WIND POWER IN SWEDEN

Analysis has been made of how the wind climate in recent decades is linked to variations in the large-scale atmospheric circulation. Also, the performance of a high-resolution climate model has been assessed. It has also been investigated how future wind conditions may change, both in the high-resolution model, but also in large ensembles of global and regional climate model simulations. In addition, an energy systems model has been applied to investigate how a future energy system including an increased fraction of wind power could be optimized to handle variations in wind between years. The results show that the variability in the historical wind climate can be linked to the large-scale atmospheric circulation and that this can be used to categorize different years, both in terms of total wind resource and conditions for periods with low wind speeds.

Energiforsk is the Swedish Energy Research Centre – an industrially owned body dedicated to meeting the common energy challenges faced by industries, authorities and society. Our vision is to be hub of Swedish energy research and our mission is to make the world of energy smarter.